Electronic Supplementary Material (ESI) for ChemComm.

Supporting Information

Biaryl sulfonamides as *cisoid* azosters for photopharmacology

Piermichele Kobauri,[a] Wiktor Szymanski,*[b] Fangyuan Cao,[c] Sebastian Thallmair,[d,e] Siewert J. Marrink,[d] Martin D. Witte,[f] Frank J. Dekker*[c] and Ben L. Feringa*[a]

[a] Stratingh Institute for Chemistry, University of Groningen, Nijenborgh 4, 9747 AG, Groningen, The Netherlands

[b] Medical Imaging Center, University of Groningen, University Medical Center Groningen, Hanzeplein 1, 9713 GZ, Groningen, The Netherlands

[c] Chemical and Pharmaceutical Biology, Groningen Research Institute of Pharmacy, University of Groningen, A. Deusinglaan 1, 9713 AV Groningen, The Netherlands

[d] Groningen Biomolecular Sciences and Biotechnology Institute & Zernike Institute for Advanced Materials, University of Groningen, Nijenborgh 7, 9747 AG Groningen, The Netherlands

[e] Frankfurt Institute for Advanced Studies, Ruth-Moufang-Straße 1, 60438 Frankfurt am Main, Germany

[f] Chemical Biology II, Stratingh Institute for Chemistry, University of Groningen, 9747AG Groningen, The Netherlands

Table of contents

S1. Synthesis and Characterization

S1.1. General remarks

Synthesis and isolation of compounds. All chemicals for synthesis were obtained from commercial suppliers (Sigma-Aldrich, Combi-blocks, and Boom) and used as received, unless stated otherwise. Solvents used were reagent grade for synthesis and technical grade for isolation if not otherwise stated. Thin layer chromatography was carried out on aluminum sheets coated with silica gel 60 F254 (Merck). The developed chromatogram was analyzed by UV lamp (254 nm) for the detection of components. Alternatively, oxidative staining using aqueous basic potassium permanganate solution ($KMnO_4$) or aqueous acidic cerium phosphomolybdic acid solution (Seebach's stain) were used. Flash chromatography was performed on silica gel (Screening devices B.V.) with a particle size of 40−64 μM and a pore size of 60 Å or on Buchi FlashPure silica columns (4-25 g, 40−63 μM, 60 Å) using a Buchi Reveleris® X2 system.

Compound characterization. Nuclear magnetic resonance (NMR) spectra were recorded on an Agilent Technologies 400-MR (400/54 Premium Shielded) spectrometer (400 MHz). All spectra were measured at room temperature (22-24 °C). Chemical shifts for the specific NMR spectra were reported relative to the residual solvent peak in ppm (δ_H = 7.26 and δ_C = 77.16 for $CDCl_3$; δ_H = 2.49 and δ_C = 39.5 for d_6-DMSO]. The multiplicities of the signals are denoted by: s (singlet), d (doublet), t (triplet), q (quartet), m (multiplet), br (broad). All ^{13}C-NMR spectra are ^{1}H-broadband decoupled. High-resolution mass spectrometry was performed on a Thermo scientific LTQ Orbitrap XL in positive (ACPI/ESI) or negative (ESI) mode. Melting point ranges were determined on a Stuart analogue capillary melting point SMP11 apparatus.

S1.2. Synthetic schemes

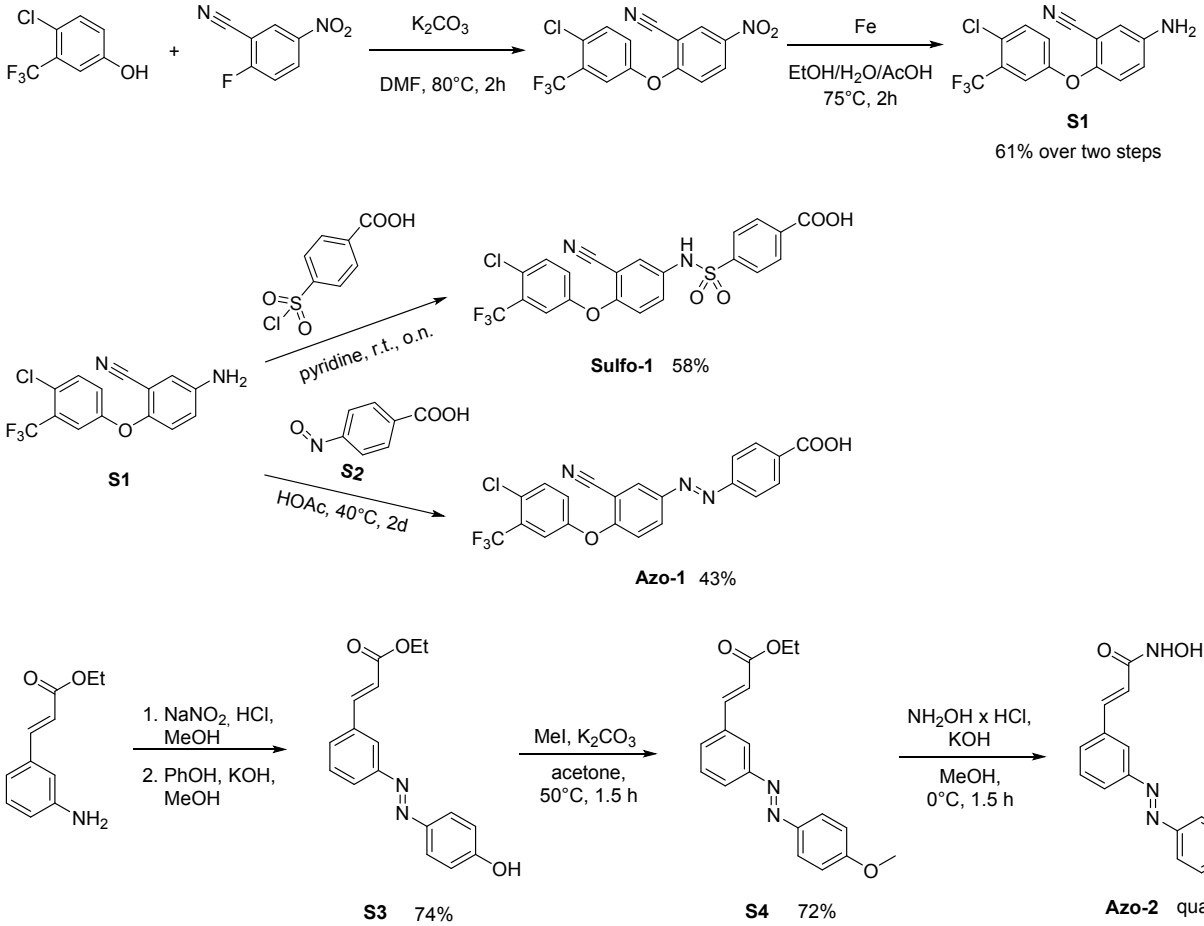

S1.3. Synthetic procedures

5-amino-2-(4-chloro-3-(trifluoromethyl)phenoxy)benzonitrile (S1)

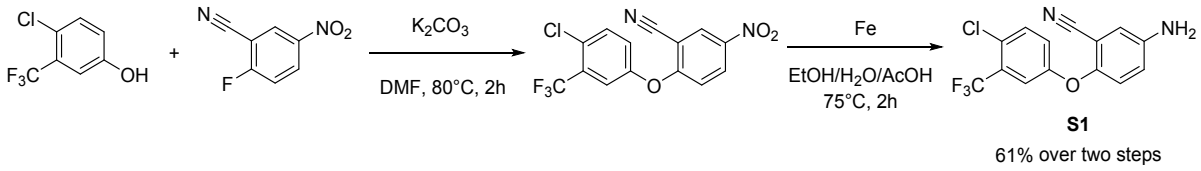

Prepared following a literature procedure.[1]

Step A: 2-fluoro-5-nitrobenzonitrile (15.5 mmol, 3.04 g) was dissolved in DMF, then K_2CO_3 (20.1 mmol, 2.78 g) and 4-chloro-3-(trifluoromethyl)phenol (15.5 mmol, 2.57 g) were added to the mixture, which was heated at 80 °C for 2 h. The reaction was quenched with water, and the product was extracted with EtOAc (3 x 40 ml). The organic phase was washed with brine (3 x 40 ml), dried over anhydrous $MgSO_4$, and the solvent was evaporated in vacuo. The residue (2-(4-chloro-3-(trifluoromethyl)phenoxy)-5-nitrobenzonitrile, 15.5 mmol, 5.30 g) was used immediately in the next step without purification.

Step B: The residue (15.5 mmol, 5.30 g) obtained from Step A was dissolved in EtOH:H_2O:AcOH (v:v:v = 10:10:1). After the addition of reduced iron powder (77.3 mmol, 4.23 g), the solution was heated to 75 °C for 2 h. Then, the reaction mixture was extracted with EtOAc (3 x 40 ml). The organic phase was washed with brine (3 x 40 ml), dried over anhydrous $MgSO_4$, and the solvent was evaporated in vacuo. The residue was purified by flash chromatography (Pentane/EtOAc = 9:1, v/v). Yield: 61% (over two steps); light pink solid. R_f: 0.3 (Pentane/EtOAc = 8:2, v/v). ^{1}H NMR (400 MHz, DMSO-d_6) δ 7.69 (d, *J* = 8.9 Hz, 1H), 7.39 (d, *J* = 3.0 Hz, 1H), 7.21 (dd, *J* = 8.9, 3.0 Hz, 1H), 7.05 (d, *J* = 8.5 Hz, 1H), 6.96 – 6.88 (m, 2H), 5.61 (s, 2H); HRMS (ESI$^+$) *m/z* calc. for $[M+H]^+$ ($C_{14}H_9ClF_3N_2O^+$): 313.0350, found: 313.0351. M.p.: 74-75 °C.

4-(N-(4-(4-chloro-3-(trifluoromethyl)phenoxy)-3-cyanophenyl)sulfamoyl)benzoic acid (Sulfo-1)

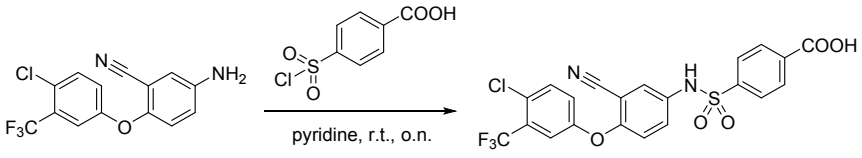

S1 **Sulfo-1** 58%

Prepared following a literature procedure[1]. **S1** (0.320 mol, 100 mg) was dissolved in pyridine, and 4-(chlorosulfonyl)benzoic acid (0.358, 79.0 mg) was added slowly. The mixture was stirred overnight at room temperature, concentrated in vacuo, and neutralized with 2 M aq. HCl. Then it was extracted with EtOAc (3 x 20 ml). The combined organic layers were washed with brine (3 x 20 ml), dried over $MgSO_4$, filtered, and concentrated under reduced pressure. Purification by flash chromatography (DCM/MeOH/AcOH = 49:1:0.05, v/v) afforded the desired compound. Yield: 59%, white solid. R_f: 0.23 (DCM/MeOH/AcOH = 49:1:0.05, v/v). ^{1}H-NMR (400 MHz, DMSO-d_6) δ 8.07 (d, *J* = 8.6 Hz, 1H), 7.85 (d, *J* = 8.5 Hz, 1H), 7.74 (d, *J* = 8.8 Hz, 1H), 7.58 (d, *J* = 2.9 Hz, 1H), 7.49 (d, *J* = 2.7 Hz, 1H), 7.39 (dd, *J* = 8.8, 3.0 Hz, 1H), 7.30 (dd, *J* = 9.1, 2.7 Hz, 1H), 7.06 (d, *J* = 9.1 Hz, 1H), spectrum in agreement with literature data[1]. HRMS (ESI$^-$) *m/z* calc. for $[M-H]^-$ ($C_{21}H_{11}ClF_3N_2O_5S^-$): 495.0035, found: 495.0031. M.p. (dec.): at 215 °C.

4-nitrosobenzoic acid (S2)

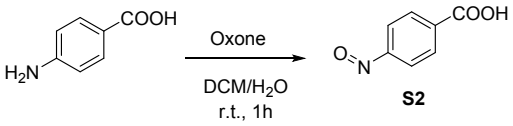

Prepared following a literature procedure.[2] To a solution of 4-aminobenzoic acid (300 mg, 2.19 mmol) in DCM (4 mL), an aqueous solution of Oxone (2.89 g in 11 mL H_2O, 4.70 mmol) was added and the suspension vigorously stirred at rt for 1 h. The precipitated product was isolated by filtration, washed with H_2O and dried. The yellow solid (crude yield = 82%) was used directly for the next step without purification.

(E)-4-((4-(4-chloro-3-(trifluoromethyl)phenoxy)-3-cyanophenyl)diazenyl)benzoic acid (Azo-1)

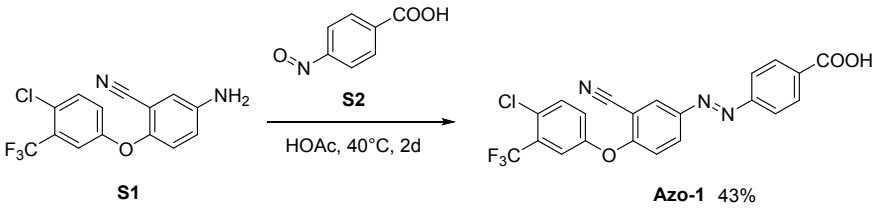

S1 (0.480 mol, 150 mg) and **S2** (0.979 mmol, 148 mg) were dissolved in AcOH (15 ml) and DMSO (15 ml). The mixture was stirred at 40 °C for 48 h. The product was isolated by filtration, washed with water, and purified by flash chromatography (DCM/MeOH, 99:1, v/v). Yield: 43%; orange solid. R_f: 0.23 (DCM:MeOH, 98:2, v/v). ^{1}H-NMR (400 MHz, DMSO-d_6) δ 13.16 (br, 1H), 8.49 (d, J = 2.5 Hz, 1H), 8.21 – 8.11 (m, 3H), 8.00 – 7.94 (m, 2H), 7.91 – 7.84 (m, 2H), 7.67 (dd, J = 8.8, 2.9 Hz, 1H), 7.27 (d, J = 9.1 Hz, 1H). ^{13}C NMR (101 MHz, DMSO-d_6) δ 166.6, 160.5, 153.9, 153.1, 147.4, 147.4, 133.9, 133.5, 130.7, 129.2, 129.0, 128.6 (q, *J* = 31.7 Hz), 127.4 (q, *J* = 2.0 Hz), 126.0, 123.6 (q, J = 273.6 Hz), 122.7, 120.3 (q, *J* = 5.5 Hz), 118.1, 115.0, 103.9. HRMS (APCI$^+$) *m/z* calc. for [M+H]$^+$ ($C_{21}H_{12}ClF_3N_3O_3^+$): 446.0514, found: 446.0530. M.p.: 200-201 °C.

Ethyl (*E*)-3-(3-((*E*)-(4-hydroxyphenyl)diazenyl)phenyl)acrylate (S3)

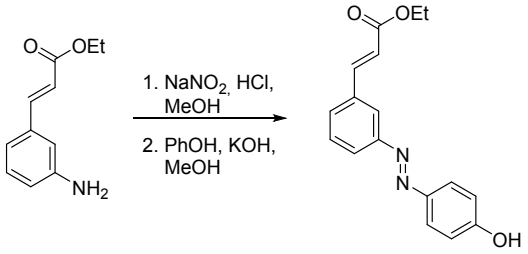

S3 74%

Ethyl 3-aminocinnamate (1.00 mmol, 191 mg) was dissolved in MeOH (1.5 mL) and 1N aq. HCl (3 mL) and the solution was cooled in an ice-water bath. A solution of $NaNO_2$ (1.20 mmol, 83 mg) in water (0.65 mL) was added, and the reaction mixture was allowed to warm up to rt, stirred for 10 min, again cooled in an ice-water bath, and added drop-wise to a solution of phenol (0.90 mmol, 85 mg) and KOH (2.0 mmol, 112 mg) in MeOH (2.5 mL). The cooling was removed. After 5 h of stirring, the reaction mixture was diluted with EtOAc (30 mL) and washed with 1M aq. HCl (3 x 20 mL) and brine (20 mL). The organic phase was dried ($MgSO_4$) and the solvent was evaporated. The product **S3** was purified by precipitation from Et_2O/pentane. Yield: 74%; orange solid. ^{1}H-NMR ($CDCl_3$, 400 MHz) δ: 8.05 (s, 1H), 7.85–7.95 (m, 3H), 7.77 (d, *J* = 16.0 Hz, 1H), 7.58 (d, *J* = 8.0 Hz, 1H), 7.52 (t, *J* = 8.0 Hz, 1H), 7.00 (d, *J* = 8.8 Hz, 2H), 6.55 (d, *J* = 16.0 Hz, 1H), 4.30 (q, *J* =7.2 Hz, 2H), 1.36 (t, *J* = 7.2 Hz, 3H); spectrum in agreement with literature data.[3]

Ethyl (*E*)-3-(3-((*E*)-(4-methoxyphenyl)diazenyl)phenyl)acrylate (S4)

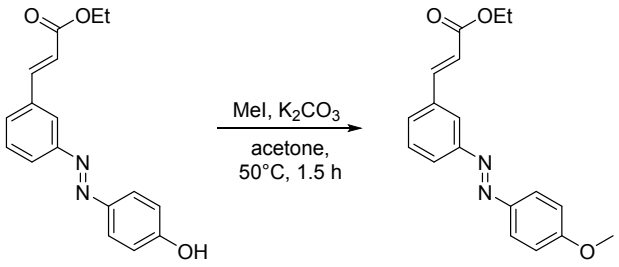

S3 74% **S4** 72%

S3 (0.67 mmol, 200 mg) was dissolved in acetone (10 mL). Methyl iodide (5.4 mmol, 334 µL) and K_2CO_3 (7.0 mmol, 966 mg) were added, and the reaction mixture was stirred at 50 ºC for 4 h. The volatiles were evaporated and the reaction mixture was diluted with Et_2O (80 mL) and washed with 1M aq. HCl (2 x 60 mL), sat. aq. $NaHCO_3$ (60 mL), and brine (60 mL). The organic phase was dried ($MgSO_4$) and the solvent was evaporated. The product was purified by flash chromatography (Pentane/Et_2O, 8:2, v/v). Yield: 72%; orange oil. R_f = 0.40 (pentane/Et_2O, 4:1, v/v). ^{1}H NMR (400 MHz,

$CDCl_3$): δ 8.04 (s, 1H), 7.94 (d, *J* = 8.9 Hz, 2H), 7.90 (d, 7.8 Hz, 1H), 7.77 (d, *J* = 16.0 Hz, 1H), 7.58 (d, *J* = 7.8 Hz, 1H), 7.51 (t, *J* = 7.7 Hz, 1H), 7.03 (d, *J* = 9.0 Hz, 2H), 6.55 (d, *J* = 16.0 Hz, 1H), 4.29 (q, *J* = 7.1 Hz, 2H), 3.90 (s, 3H), 1.35 (t, *J* = 7.1 Hz, 3H); ^{13}C NMR (101 MHz, $CDCl_3$): δ 166.8, 162.4, 153.0, 146.8, 143.9, 135.5, 129.7, 129.5, 125.0, 124.3, 121.7, 119.3, 114.3, 60.6, 55.6, 14.3; HRMS (ESI+) calc. for $[M+H]^+$ ($C_{18}H_{19}N_2O_3$): 311.1390, found: 311.1390.

(*E*)-N-hydroxy-3-(3-((*E*)-(4-methoxyphenyl)diazenyl)phenyl)acrylamide (Azo-2)

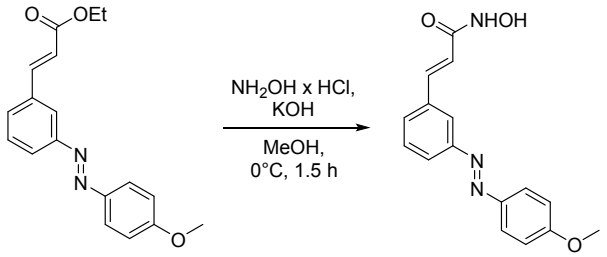

S4 72% **Azo-2** quant.

Prepared by a modification of a literature procedure for a different target.[4] Potassium hydroxide (3.90 mmol, 220 mg) was added to a solution of hydroxylamine hydrochloride (3.90 mmol, 270 mg) in dry ethanol (1.0 mL). The resulting mixture was cooled in an ice-water bath and filtered. Potassium hydroxide (0.64 mmol, 35 mg) and compound **3** (0.12 mmol, 36 mg) were added to the filtrate, and the mixture was stirred in an ice-water bath for 90 min. Water (2.5 mL) was added to the mixture, followed by 1M aq. HCl until pH<1. The resulting precipitate was filtered off and washed with EtOAc and Et_2O. After drying under vacuum, the product was obtained as orange powder (quant.). ^{1}H NMR (400 MHz, DMSO-d_6): δ 7.97 (s, 1H), 7.90 (d, *J* = 8.9 Hz, 2H), 7.80 (d, *J* = 8.0 Hz, 1H), 7.69 (d, *J* = 7.5 Hz, 1H), 7.58 (t, *J* = 7.7 Hz, 1H), 7.51 (d, *J* = 15.9 Hz, 1H), 7.13 (d, *J* = 9.0 Hz, 2H), 6.59 (d, *J* = 15.8 Hz, 1H), 3.86 (s, 3H); ^{13}C NMR (101 MHz, DMSO-d_6): δ 162.9, 162.7, 152.9, 146.6, 137.2, 136.8, 130.4, 130.2, 125.2, 123.2, 121.4, 121.0, 115.1, 56.1; HRMS (ESI+) calc. for $[M+H]^+$ ($C_{16}H_{16}N_3O_3$): 298.1187, found: 298.1186.

S2. Photochemical and Thermal Isomerization by UV-Vis and NMR Spectroscopy

S2.1. General remarks

UV-Vis absorption spectra were recorded on an Agilent 8453 UV-Visible Spectrophotometer. Photochemical isomerization (photoswitching) was achieved by irradiation from the side in a fluorescence quartz cuvette (width = 1.0 cm) using a custom-built (Prizmatix/Mountain Photonics) multi-wavelength fiber coupled LED-system (FC6-LED-WL) including the following LEDs: 365A, 390B, 420Z, 445B, 535R, 630CA. A detailed description of the setup was published by us recently.[5] A Quantum Northwest TC1 temperature controller was used to maintain the temperature at 25 °C during photochemical studies. Thermal isomerization kinetics were recorded using a JASCO V750 at 25 °C using a PTC 424S/15 temperature controller. Raw data were processed using Agilent UV-Vis ChemStation B.02.01 SP1, Spectra Manager, Spectragryph 1.2, and OriginPro 2018.

S2.2. Photoisomerization studies

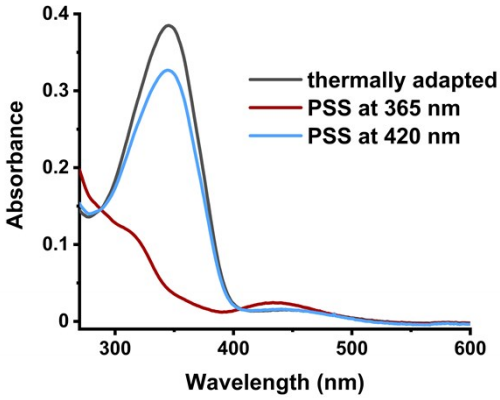

Fig. S1. Photoisomerization of **Azo-1** in DMSO (20 µM, 25 °C).

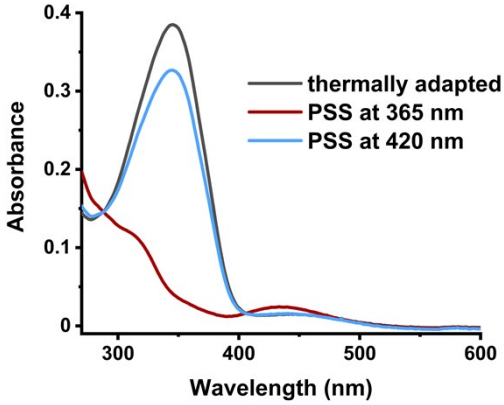

Fig. S2. Photoisomerization of **Azo-2** in DMSO (20 µM, 25 °C).

S2.3. Switching cycles for fatigue

To analyze the fatigue resistance of compounds **Azo-1**, repeated irradiation cycles were performed using alternating 365 nm and 420 nm light. For **Azo-2**, we used 390 nm and 445 nm light. The decrease and increase of the ππ* transition band was followed by UV-Vis spectroscopy (Agilent 8453) at 25 °C while stirring. The obtained data is depicted below.

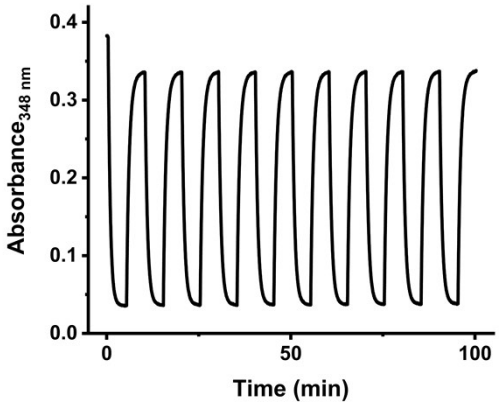

Fig. S3. Fatigue studies of **Azo-1** in DMSO (20 µM).

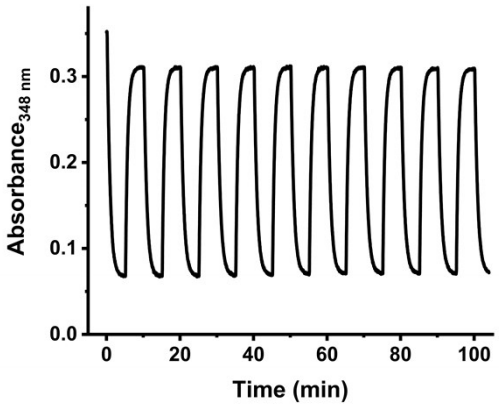

Fig. S4. Fatigue studies of **Azo-1** in Lp-PLA_2 assay buffer with 1% DMSO (20 µM).

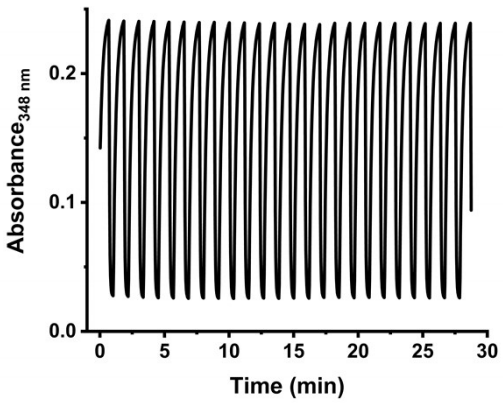

Fig. S5. Fatigue studies of **Azo-2** in HDAC2 assay buffer with 1% DMSO (20 µM).

S2.4. Determination of the thermal lifetime for the metastable cis *isomers*

Samples were irradiated with the 365-nm LED of the custom-built setup (see Section 2.1) until PSS was reached. Then, the cuvettes were placed in a JASCO V750 spectrophotometer and the recovery of the π-π* transition was followed while stirring at 25 °C. The data were fitted using a first-order exponential function in OriginPro 2018.

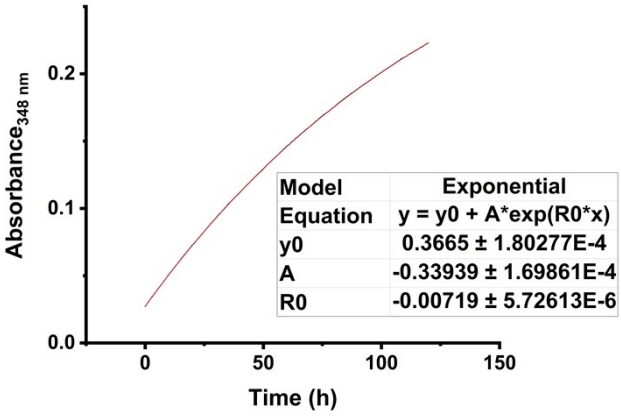

Fig. S6. Thermal *cis*-to-*trans* isomerization of **Azo-1** in DMSO (20 µM). Exponential fitting gave $t_{1/2}$ = 96 h.

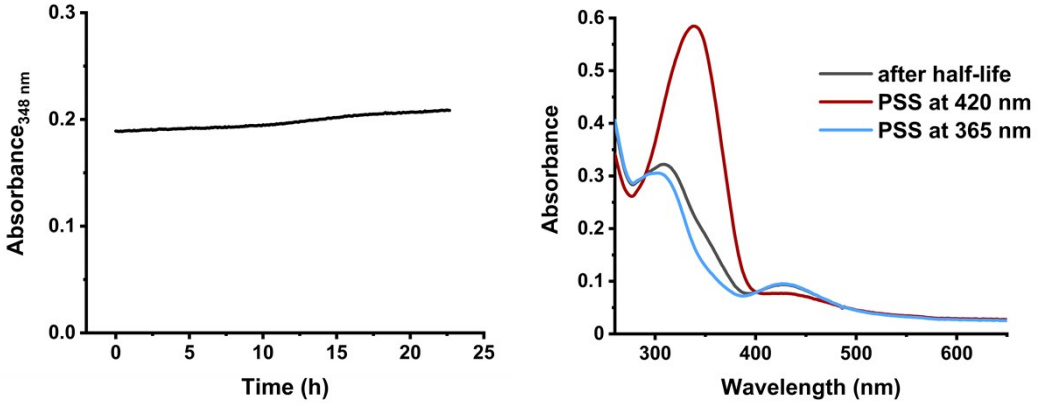

Fig. S7. (left) Thermal *cis*-to-*trans* isomerization of **Azo-1** in Lp-PLA_2 assay buffer with 1% DMSO (20 µM). Minimal back-isomerization was observed, therefore no numerical value for the half-life could be obtained. (right) After 24 h of measurement, the UV-Vis spectrum of the sample showed that it mainly consisted *cis*-**Azo-1**. This was further confirmed by irradiation with 420 nm (back-switching) and subsequent irradiation wit 365 nm (switching).

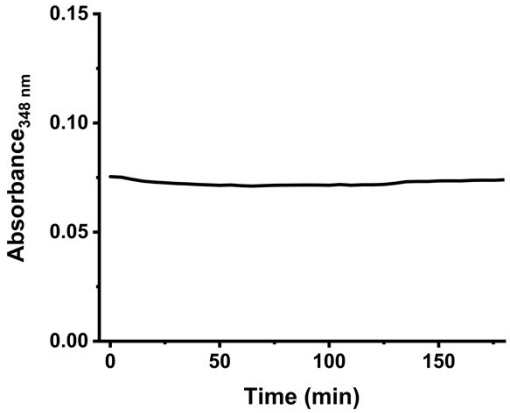

Fig. S8. Thermal *cis*-to-*trans* isomerization of **Azo-2** in HDAC2 assay buffer with 1% DMSO (20 μM). Minimal back-isomerization was observed, therefore no numerical value for the half-life could be obtained.

S2.5. PSD determination by NMR

0.5 mL of a 2 mM solution of the respective compound in DMSO-d_6 was thermally equilibrated by briefly (~10 s) heating the sample using a heat gun, or irradiated in a glass NMR tube using a 365 nm hand-held lamp (Spectroline ENB-280C) or the 420-nm LED of the custom-built setup, respectively.

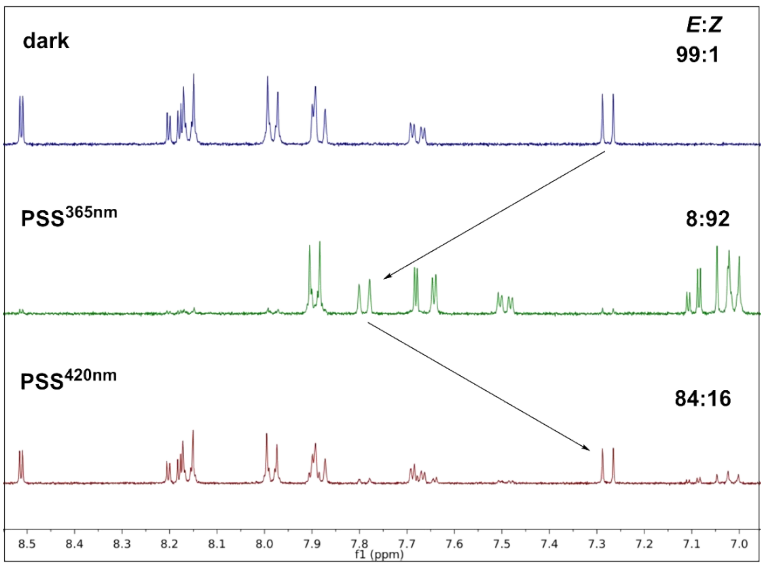

Fig. S9. Azo-1, DMSO-d_6, ~2 mM.

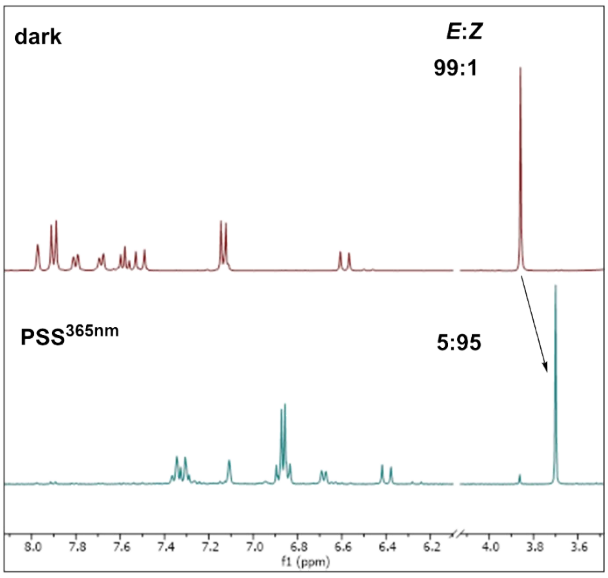

Fig. S10. Azo-2, DMSO-d_6, ~2 mM.

S2.6. Solubility measurements

To evaluate the solubility of *trans*- and *cis*-**Azo-1** up to 100 µM in Lp-PLA$_2$ assay buffer (50 mM TRIS-HCl, pH 8.0, 150 mM NaCl, 0.1 mg/mL BSA), UV-Vis spectra were recorded at different concentrations after 10 min of stirring at 25 °C.

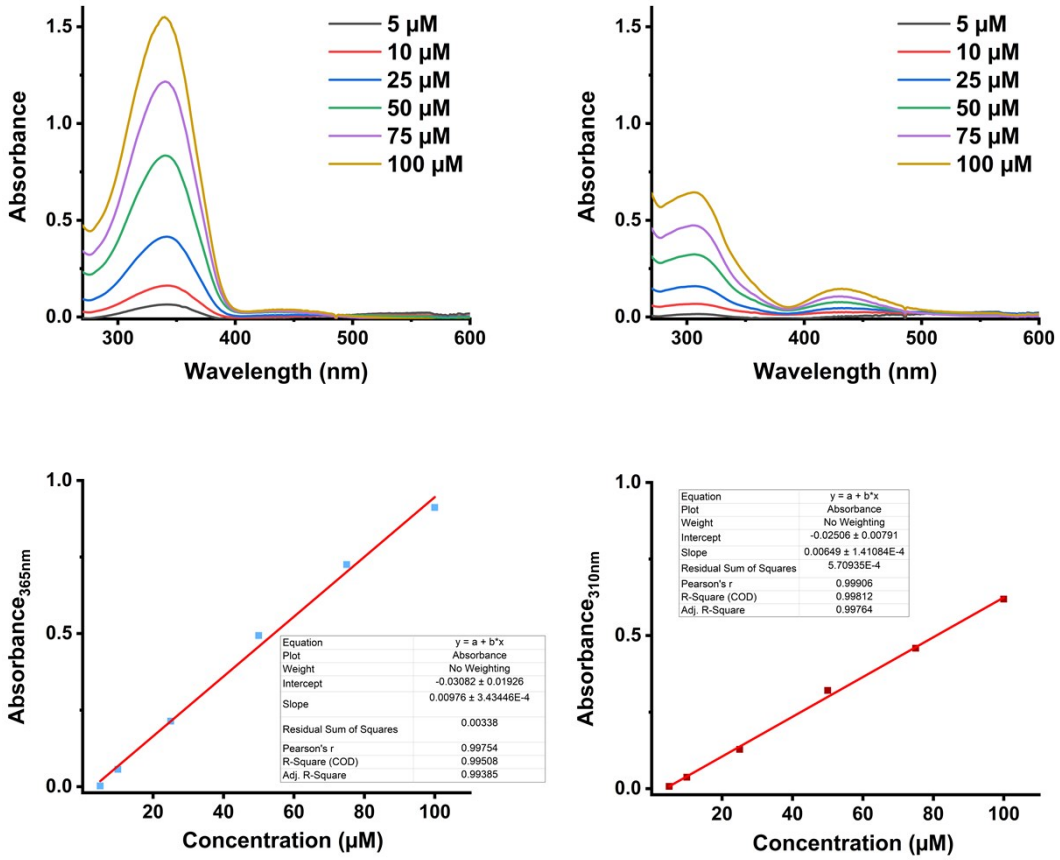

Fig. S11. (top) *trans*-**Azo-1** (left) and *cis*-**Azo-1** (right) in Lp-PLA$_2$ assay buffer with 5% DMSO. (bottom) Linear fit curve and parameters.

S3. Biological assays

S3.1. Competition experiments on Lp-PLA$_2$

Human recombinant Lipoprotein-Associated Phospholipase A_2 (Sigma-Aldrich, Catalog #: SRP3136) was diluted in assay buffer (50 mM TRIS-HCl, pH 8.0, 150 mM NaCl, 0.1 mg/mL BSA) to reach a concentration of 20 ng/µL. 9 µL enzyme solution were incubated for 30 min with inhibitor (0.5 µL, different concentrations DMSO), followed by an incubation of 30 min with PJD224[6] (0.5 µL, 20 µM). Then, reducing sample buffer (4 µL, 4x) was added and the samples were boiled at 100 °C for 15 minutes and the samples were loaded on 15% TRIS-glycine type SDS-PAGE gel according to standard literature procedures.

Gels were prepared using acrylamide-bis ready-to-use solution 40% (37.5:1) (Merck Millipore) and separated on a Mini-PROTEAN Tetra cell (Bio-Rad). In-gel fluorescence scanning of the SDS-PAGE gels was performed on a Typhoon FLA 9500 (GE Healthcare) using the Cy2-settings for BODIPY (laser excitation at 473 nm and emission filter 515-545 nm). After fluorescent scanning of the gel, the proteins were stained with a Coomassie brilliant blue R250 solution or Roti®-Blue Colloidal Coomassie staining solution (Carl Roth) according to standard protocols.

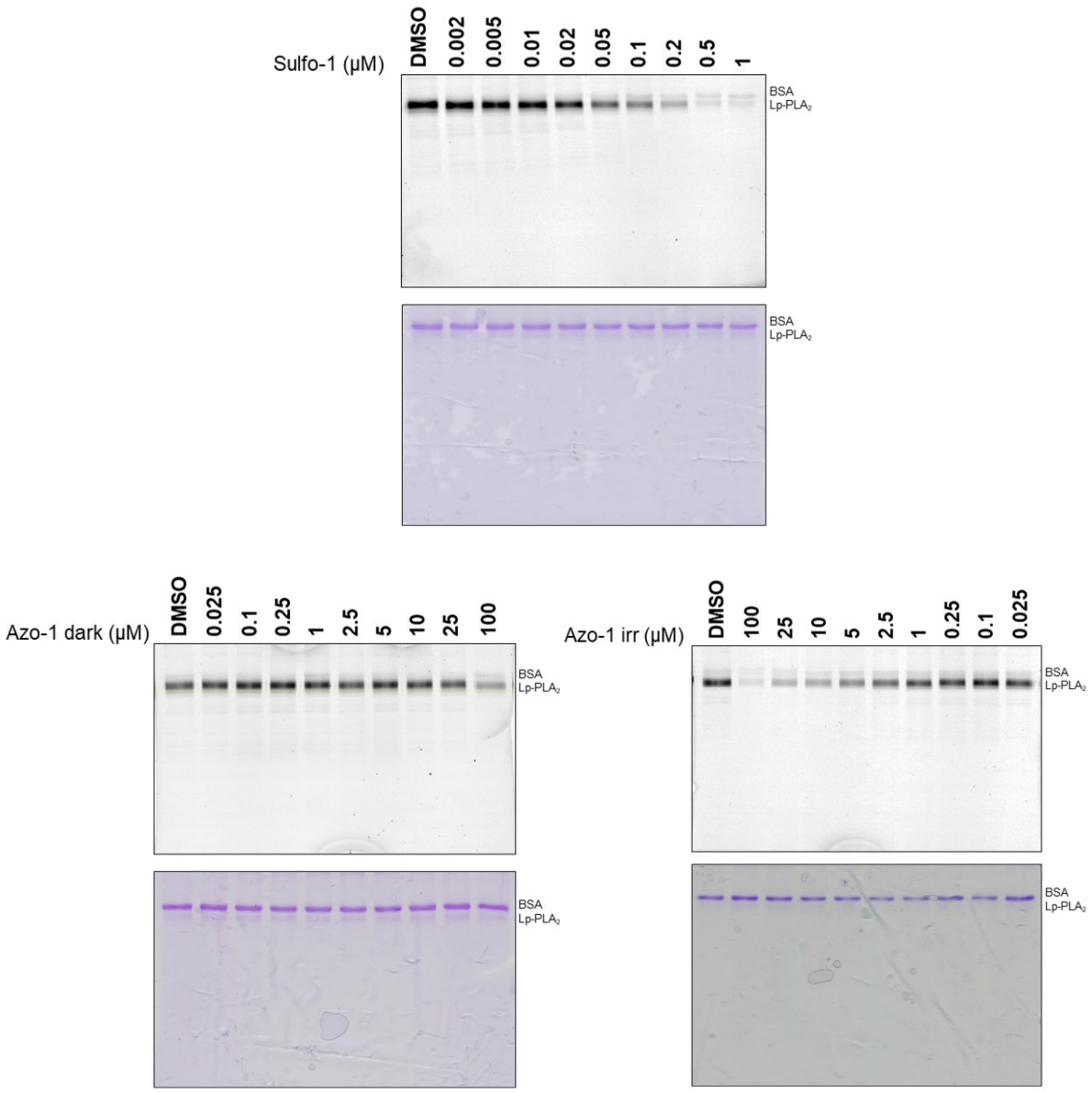

Fig. S12. First replica. The top gels are fluorescence-scanned, the bottom gels are stained with Coomassie.

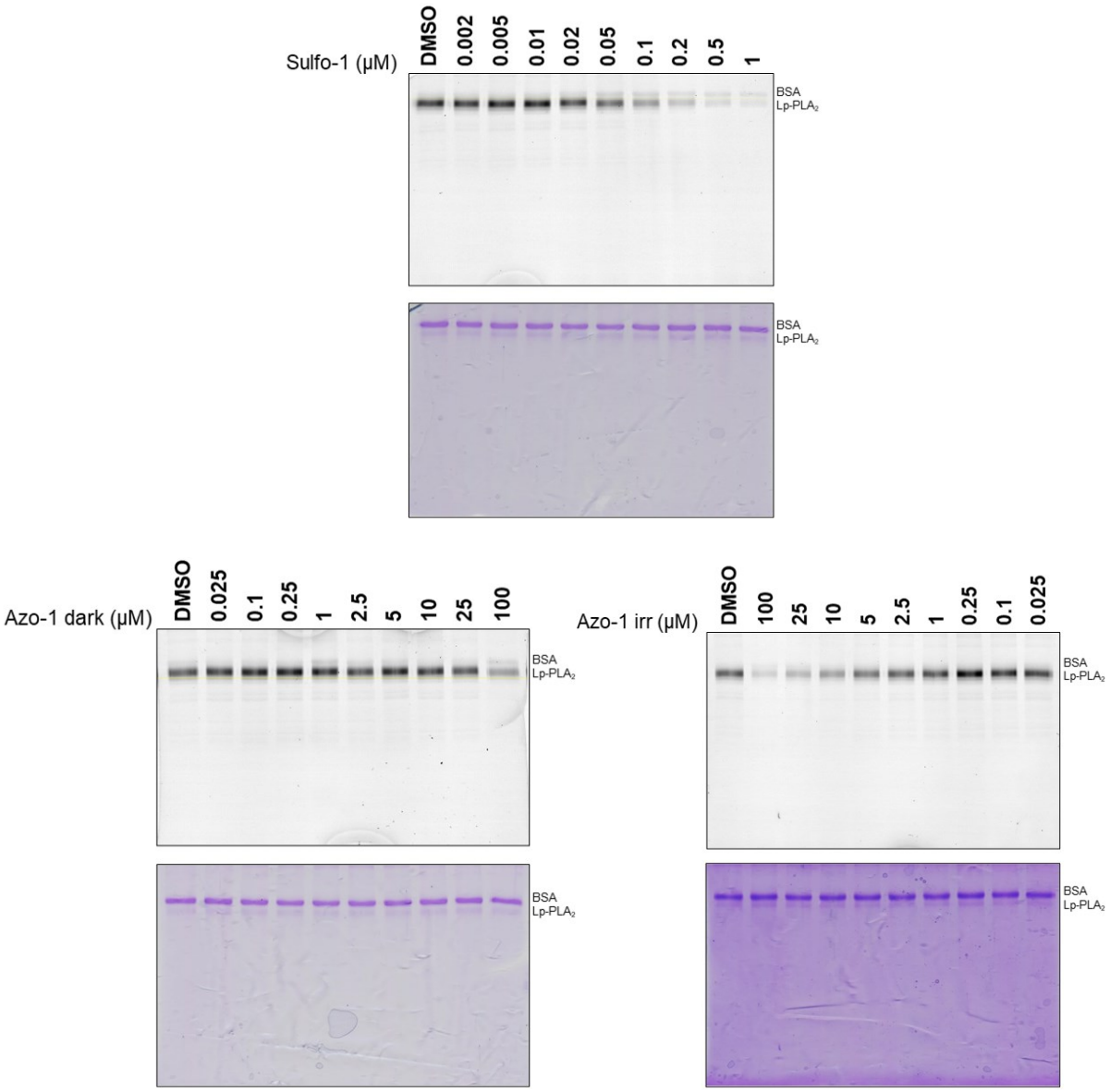

Fig. S13. Second replica. The top gels are fluorescence-scanned, the bottom gels are stained with Coomassie.

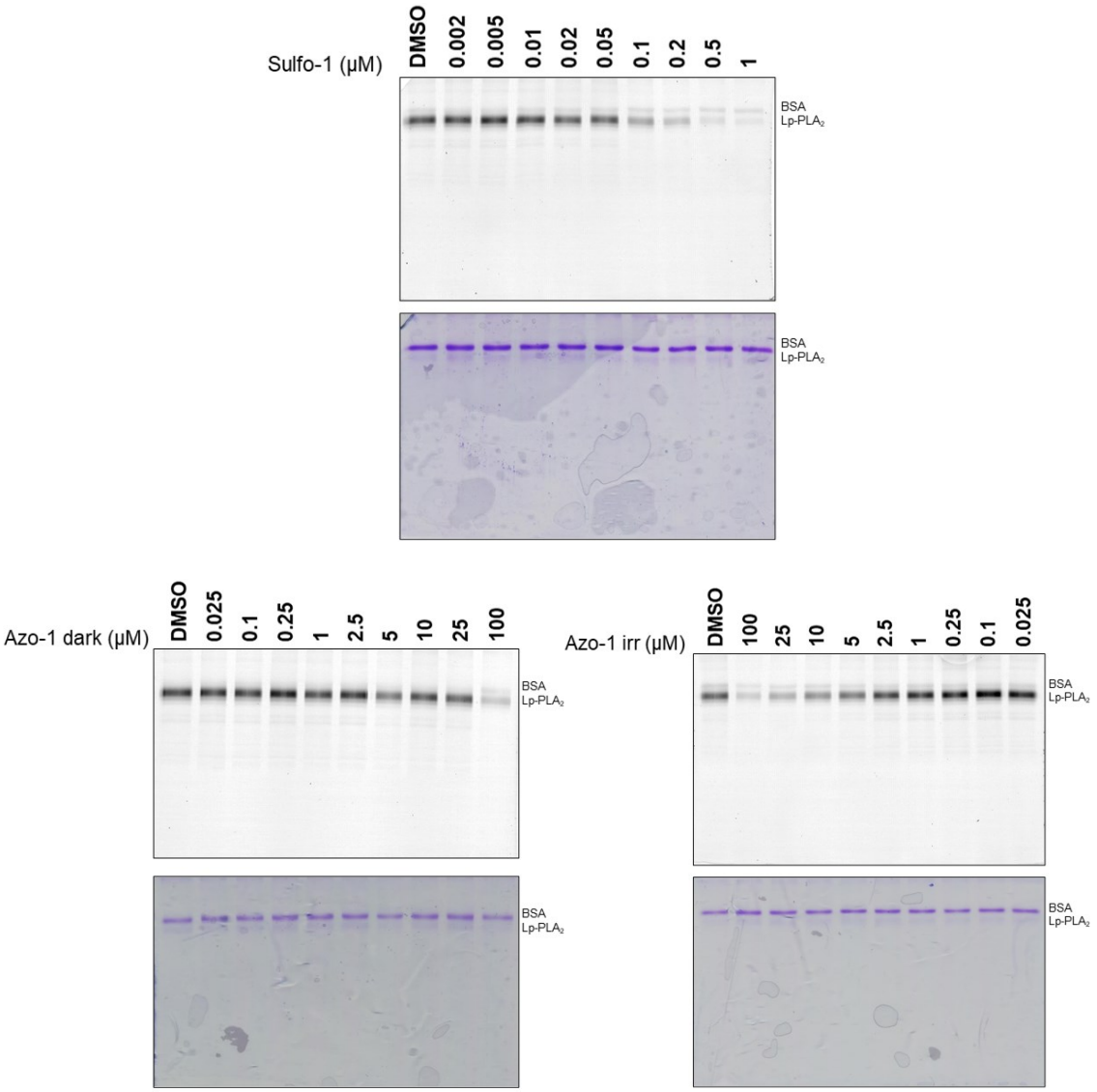

Fig. S14. Third replica. The top gels are fluorescence-scanned, the bottom gels are stained with Coomassie.

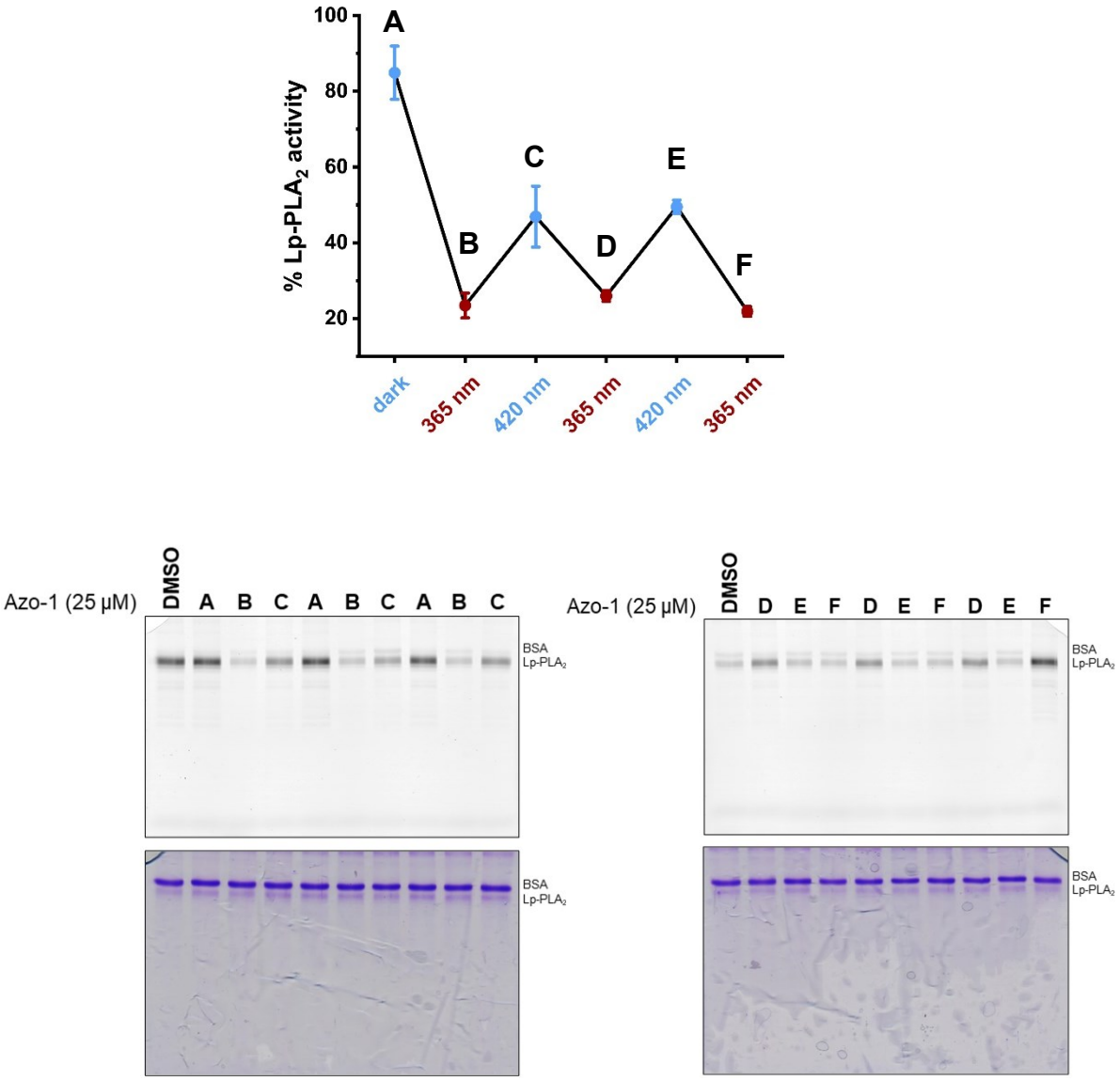

Fig. S15. Reversible control on Lp-PLA$_2$ activity at 25 μM (see Fig. 3 in the main text). Three replicas were performed per point. The top gels are fluorescence-scanned, the bottom gels are stained with Coomassie.

S3.2. HDAC2 inhibition assay

The *trans* isomer was obtained after heating the stock solution in DMSO at 60^{o}C for 5 min. The *cis* isomer was tested after 1 h irradiation of the same solution at 365 nm wavelength.

Black 96-well flat bottom microplates (Corning® Costar®, Corning Incorporated, NY) were used. Human recombinant C-terminal FLAG-tag HDAC2 (BPS Bioscience, Catalog #: 50052) was diluted in incubation buffer (25 mM Tris-HCl, pH 8.0, 137 mM NaCl, 2.7 mM KCl, 1 mM $MgCl_2$, 0.01% Triton-X and 0.1 mg/mL BSA). 40 µL of this dilution was incubated with 10 µL of different concentrations of inhibitors in 10% DMSO/incubation buffer and 50 µL of the fluorogenic Boc-Lys(ε-Ac)-AMC (20 µM, Bachem, Germany) at 37 °C. After 90 min incubation time, 50 µL of the stop solution (25 mM Tris-HCl (pH 8), 137 mM NaCl, 2.7 mM KCl, 1 mM $MgCl_2$, 0.01% Triton-X, 6.0 mg/mL trypsin from porcine pancreas Type IX-S, lyophilized powder, 13,000-20,000 BAEE units/mg protein (Sigma Aldrich) and 200 µM vorinostat) was added. After an incubation at 37 °C for 30 min, the fluorescence was measured on a Synergy H1 Hybrid Multi-Mode Microplate Reader (BioTek, USA) with a gain of 70 and an excitation wavelength of 390 nm and an emission wavelength of 460 nm. GraphPad Prism 5.0 (GraphPad Software, Inc.) was used for the determination of the IC_{50} of each inhibitor. Nonlinear regression was used for data fitting (Fig. S16). The statistical significance of the difference in activity between **Azo-2 irr** and **Azo-2 dark** was checked with the extra sum-of-squares F-test (Fig. S17).

Nonlin fit	A	B	C
	Azo-2 irr	Azo-2 dark	Sulf-2
	Y	Y	Y
1 log(inhibitor) vs. response -- Variable slope			
2 Best-fit values			
3 BOTTOM	-2.002	0.9516	-0.6409
4 TOP	99.57	94.98	98.73
5 LOGIC50	-6.623	-6.353	-7.444
6 HILLSLOPE	-0.8323	-1.182	-0.8007
7 IC50	2.384e-007	4.434e-007	3.600e-008
8 Span	101.6	94.03	99.37
9 Std. Error			
10 BOTTOM	2.183	2.598	1.848
11 TOP	0.8480	1.510	2.220
12 LOGIC50	0.03753	0.06519	0.06079
13 HILLSLOPE	0.05078	0.1540	0.08186
14 Span	2.559	3.086	3.185
15 95% Confidence Intervals			
16 BOTTOM	-6.490 to 2.485	-4.424 to 6.327	-4.440 to 3.158
17 TOP	97.83 to 101.3	91.85 to 98.10	94.17 to 103.3
18 LOGIC50	-6.700 to -6.545	-6.488 to -6.218	-7.569 to -7.319
19 HILLSLOPE	-0.9367 to -0.7279	-1.500 to -0.8631	-0.9690 to -0.6324
20 IC50	1.996e-007 to 2.848e-007	3.250e-007 to 6.049e-007	2.700e-008 to 4.801e-008
21 Span	96.32 to 106.8	87.64 to 100.4	92.83 to 105.9
22 Goodness of Fit			
23 Degrees of Freedom	26	23	26
24 R^2	0.9955	0.9828	0.9871
25 Absolute Sum of Squares	187.0	735.7	662.4
26 Sy.x	2.682	5.656	5.047
27 Number of points			
28 Analyzed	30	27	30

Fig. S16. Nonlinear fitting of inhibition data of **Azo-2 irr**, **Azo-2 dark** and **Sulf-2**.

Nonlin fit	A	B	C
	Azo-2 irr	Azo-2 dark	Global (shared)
	Y	Y	Y
Comparison of Fits			
Null hypothesis			LOGIC50 same for all data sets
Alternative hypothesis			LOGIC50 different for each data set
P value			0.0028
Conclusion (alpha = 0.05)			Reject null hypothesis
Preferred model			LOGIC50 different for each data set
F (DFn, DFd)			9.930 (1,49)
LOGIC50 different for each data set			
Best-fit values			
BOTTOM	-2.002	0.9516	
TOP	99.57	94.98	
LOGIC50	-6.623	-6.353	
HILLSLOPE	-0.8323	-1.182	
IC50	2.384e-007	4.434e-007	
Span	101.6	94.03	
Std. Error			
BOTTOM	2.183	2.598	
TOP	0.8480	1.510	
LOGIC50	0.03753	0.06519	
HILLSLOPE	0.05078	0.1540	
Span	2.559	3.086	
95% Confidence Intervals			
BOTTOM	-6.490 to 2.485	-4.424 to 6.327	
TOP	97.83 to 101.3	91.85 to 98.10	
LOGIC50	-6.700 to -6.545	-6.488 to -6.218	
HILLSLOPE	-0.9367 to -0.7279	-1.500 to -0.8631	
IC50	1.996e-007 to 2.848e-007	3.250e-007 to 6.049e-007	
Span	96.32 to 106.8	87.64 to 100.4	
Goodness of Fit			
Degrees of Freedom	26	23	
R^2	0.9955	0.9828	
Absolute Sum of Squares	187.0	735.7	
Sy.x	2.682	5.656	
LOGIC50 same for all data sets			
Best-fit values			
BOTTOM	-11.93	2.468	
TOP	99.86	95.53	
LOGIC50	-6.438	-6.438	-6.438
HILLSLOPE	-0.6936	-1.179	
IC50	3.651e-007	3.651e-007	3.651e-007
Span	111.8	93.06	
Std. Error			
BOTTOM	3.909	2.073	
TOP	1.616	1.247	
LOGIC50	0.04777	0.04777	0.04777
HILLSLOPE	0.06472	0.1225	
Span	4.910	2.517	
95% Confidence Intervals			
BOTTOM	-19.79 to -4.068	-1.700 to 6.635	
TOP	96.61 to 103.1	93.02 to 98.04	
LOGIC50	-6.534 to -6.342	-6.534 to -6.342	-6.534 to -6.342
HILLSLOPE	-0.8237 to -0.5635	-1.425 to -0.9327	
IC50	2.927e-007 to 4.555e-007	2.927e-007 to 4.555e-007	2.927e-007 to 4.555e-007
Span	101.9 to 121.7	88.00 to 98.12	
Goodness of Fit			
Degrees of Freedom			50
R^2	0.9922	0.9816	0.9868
Absolute Sum of Squares	322.1	787.6	1110
Sy.x			4.711
Constraints			
LOGIC50	LOGIC50 is shared	LOGIC50 is shared	
Number of points			
Analyzed	30	27	

Fig. S17. Results of the extra sum-of-squares F test for **Azo-2 irr** and **Azo-2 dark**.

S4. Molecular modeling

S4.1. General remarks

The calculations and analysis were performed either on a HP EliteDesk, with an Intel Core i7-6700 processor with four cores and an NVIDIA GeForce GTX 1060 3GB graphics card (Geometry measurements and Molecular docking), or on the Peregrine cluster at the University of Groningen (Molecular Dynamics and DFT calculations).

The substructure search in the CSD was performed on ConQuest (as of July 2020, ver 2.0.5, Cambridge Crystallographic Data Centre), and the measurements were handled through Mercury (ver 4.3.1, Cambridge Crystallographic Data Centre) and Excel 2019 (Microsoft). The substructure search in the PDB was carried out on https://www.rcsb.org/pdb/ligand/chemAdvSearch.do (as of April 2020) and processed with KNIME (ver 4.1.1, KNIME AG, Zurich, Switzerland), using Schrödinger nodes and a custom Python script (based on the measure_by_smarts.py script) provided by Schrödinger. The histograms were generated with Jupyter-notebook, using Matplotlib.

The docking calculations, the molecular dynamics simulations and the DFT calculations were carried out with Maestro (ver 12.4, Schrödinger Release 2020-2: Maestro, Schrödinger, LLC, New York, NY, 2020).

S4.2. Geometry measurements from the CSD

All ring atoms were set as “any” to allow all possible heterocycles and substitutions, and the two linker atoms were set as “acyclic”. Two substructures were queried on ConQuest:

1. Azobenzene:

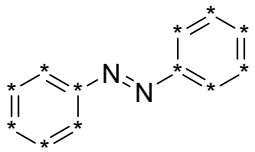

2. Any potential azostere with a generic two-atom linker and excluding substructure 1:

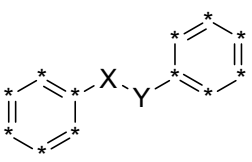

CSD search parameters: 3D coordinates determined, R factor ≤ 0.10, only not disordered, no errors, not polymeric, no ions, only organic.

1291 azobenzene and 28602 generic azostere structures were found (the count includes all multiple fragments of the CSD entries). The following geometric features were measured:

- Dihedral angle around the X-Y bond (aXYa);

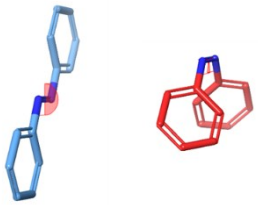

- Centroid angle (the angle formed by the centroid of the first ring, the centroid of the XY bond, and the centroid of the second aromatic ring);

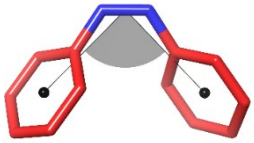

- Ring distance (the distance between the centroids of the two aromatic rings);

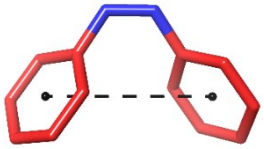

- Ring angle (the angle formed by the planes of the two aromatic rings).

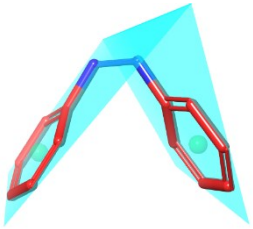

The criterion to divide the dataset into *trans* and *cis* was the cNNc dihedral angle measured for the azobenzene query. Azobenzene structures were considered to be *cis*-azobenzene with -50° ≤ cNNc ≤ 50°, resulting in 1238 trans-azobenzene and 53 cis-azobenzene entries. The comparison of the distributions of *trans*-, *cis*-azobenzene and the generic system (Fig. S18) showed that three additional geometric criteria describe the similarity to *cis*-azobenzene:

1. centroid angle < 100°;
2. ring distance < 5 Å;
3. ring angle > 50°.

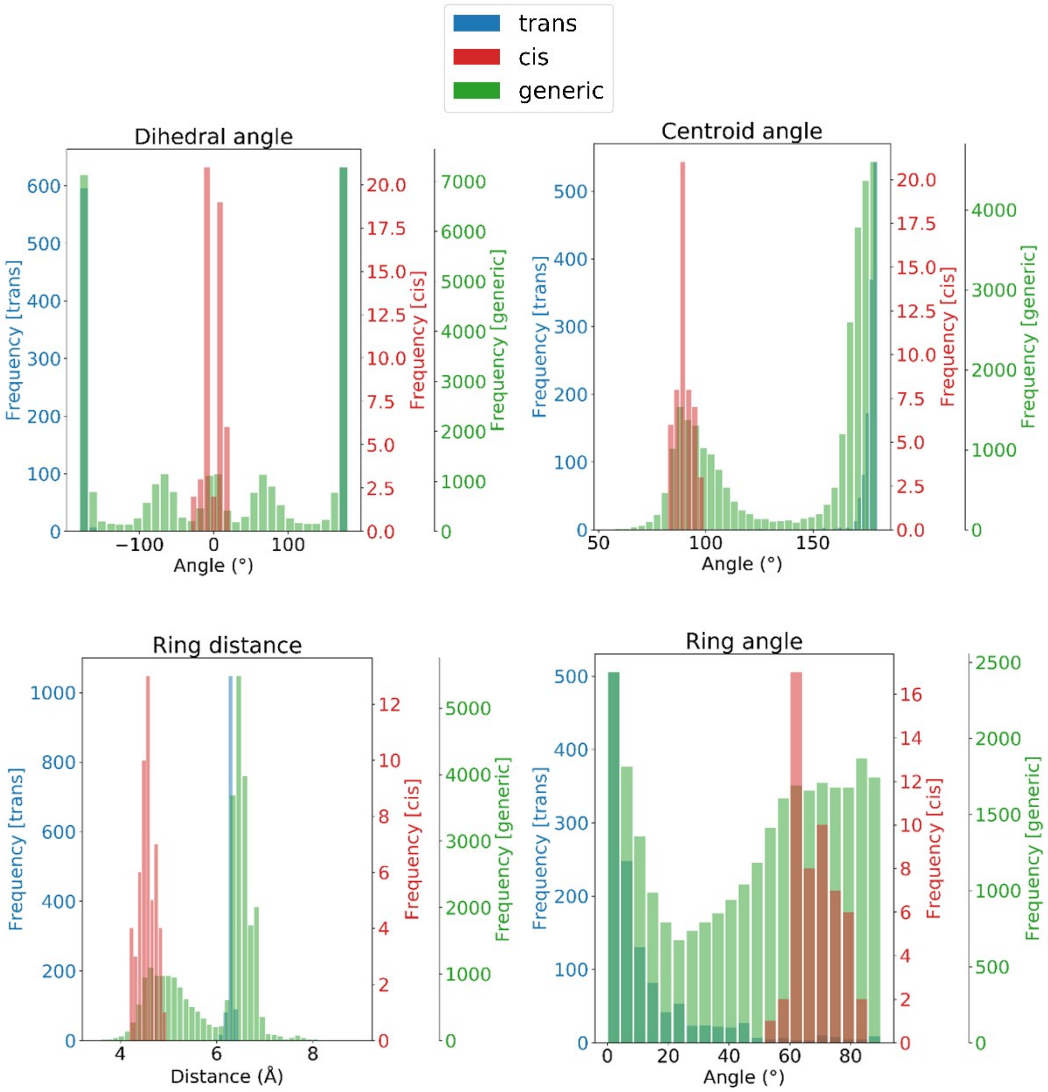

Fig. S18. Distributions of dihedral angles, centroid angles, ring distances and ring angles of the generic azostere, *trans*- and *cis*-azobenzene in the CSD.

Based on the centroid angle criterium, three substructures were selected as *cisoid*.

Entry	Substructure	Hits	*Transoid*	*Cisoid*
Biaryl sulfonamide	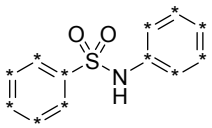	1121	0	863
N-Benzylaniline	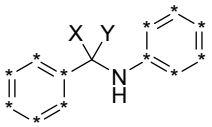	1364	391	345
N-Benzyl-*N*-methylaniline	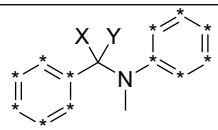	38	3	13
N-Methylbenzanilide	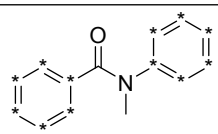	154	16	137

Table S1. *Cisoid* structures found in the CSD. *Transoid* populations are defined as having centroid angle > 150°.

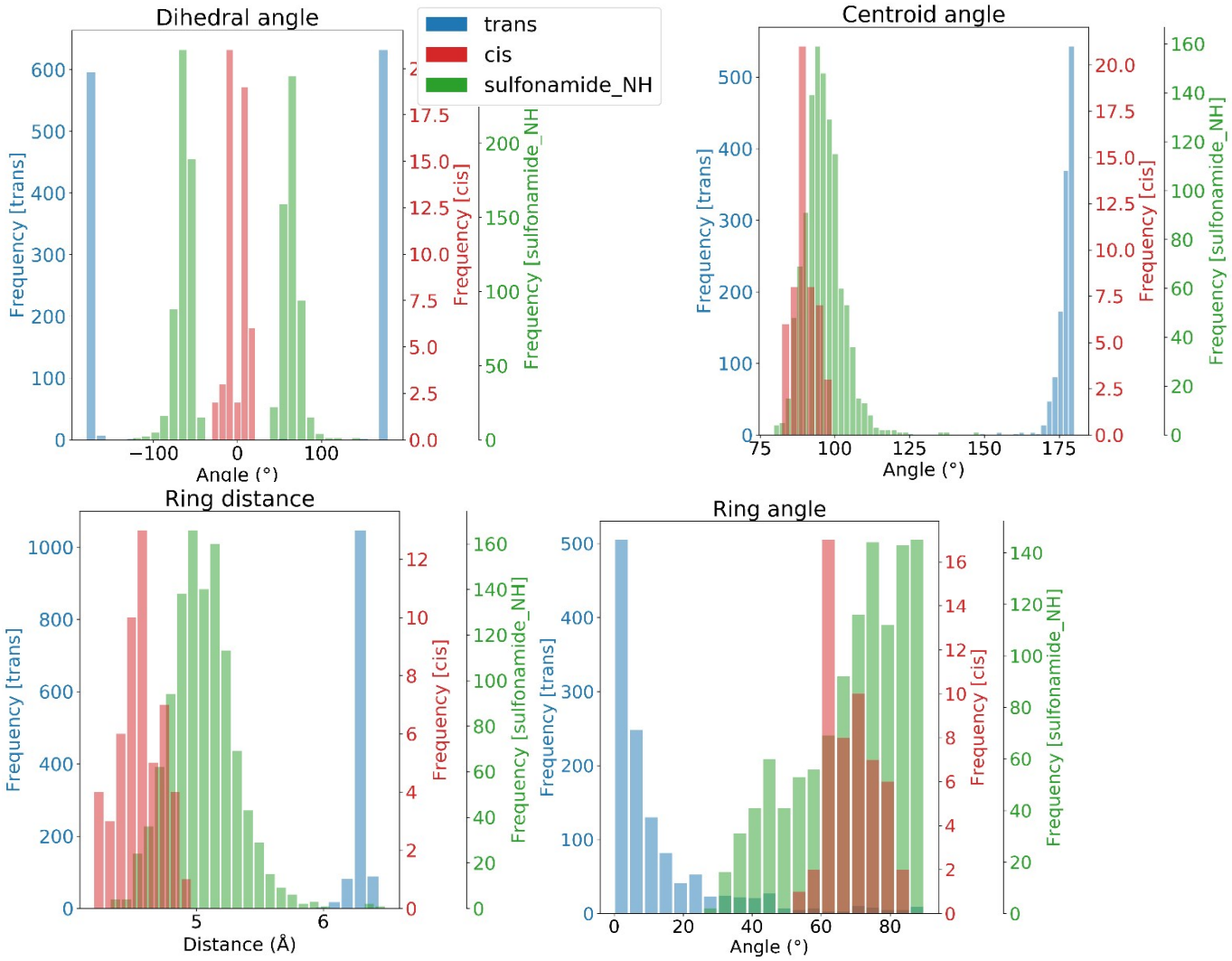

Fig. S19. Distributions of dihedral angles, centroid angles, ring distances and ring angles of biaryl sulfonamide, *trans*- and *cis*-azobenzene structures in the CSD.

N-unsubstituted biaryl sulfonamides showcase a *cisoid* geometry in more than 75% of the structures, according to the centroid angle criterium. However, when dihedral angles are considered, most of the biaryl sulfonamides in the CSD appear to have a non-suitable dihedral angle being between the values observed for *cis*- and *trans*-azobenzene structures.

On the other hand, *N*-benzylanilines adopt both *cisoid* and *transoid* conformations. *N*-methylation slightly favors *cisoid N*-benzylanilines, while it is needed for benzanilides to be *cisoid* (Fig. S20 and S21). This requirement not only tightens the chemical space of ligands to be considered for azologization, but also has an influence on the electronic similarity of the azostere with *cis*-azobenzene (see section S4.6).

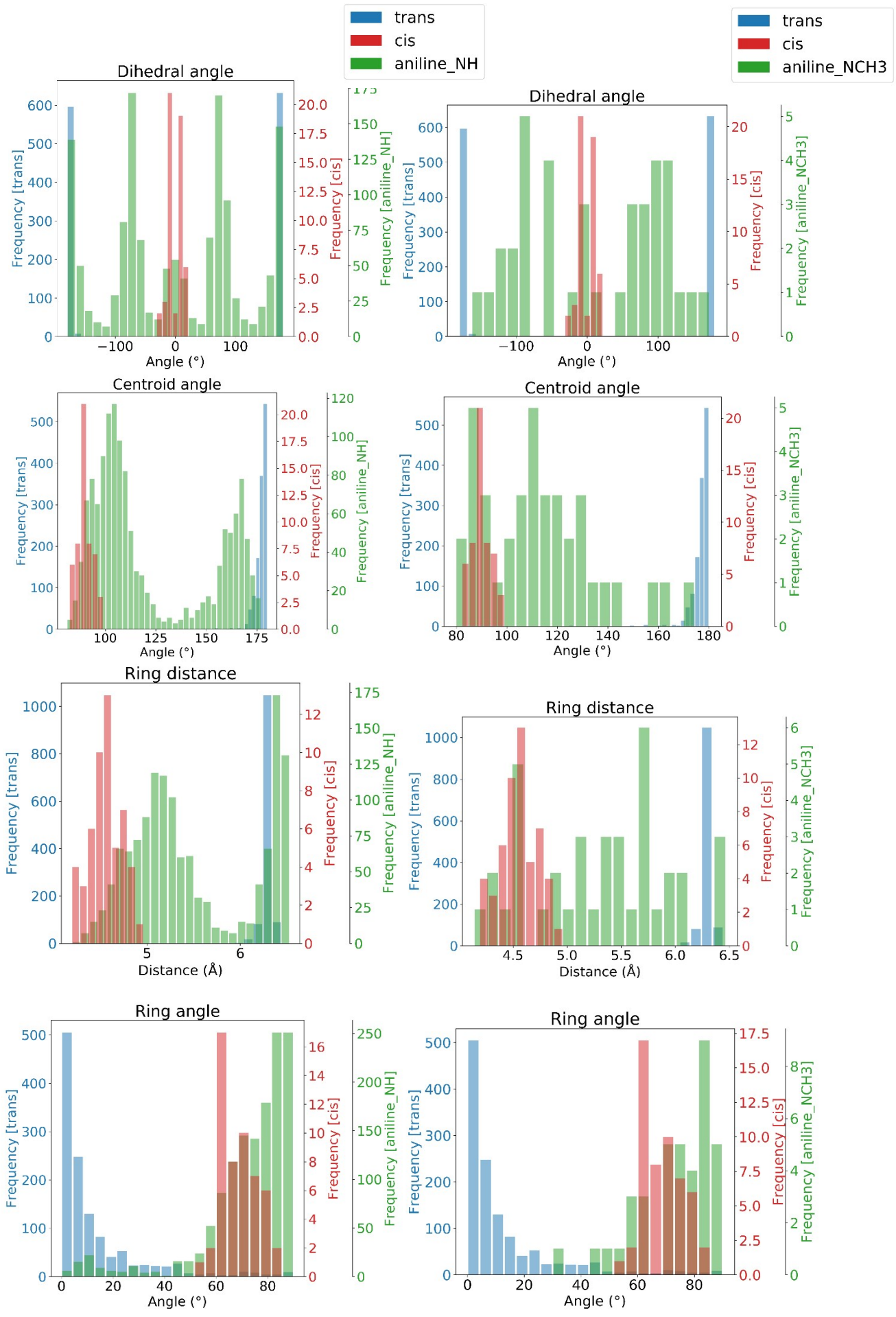

Fig. S20. Geometric distributions for *N*-unsubstitued (left, data from 1364 structures) and *N*-methyl (right, data from 38 structures) *N*-benzylaniline, *trans*- and *cis*-azobenzene structures in the CSD.

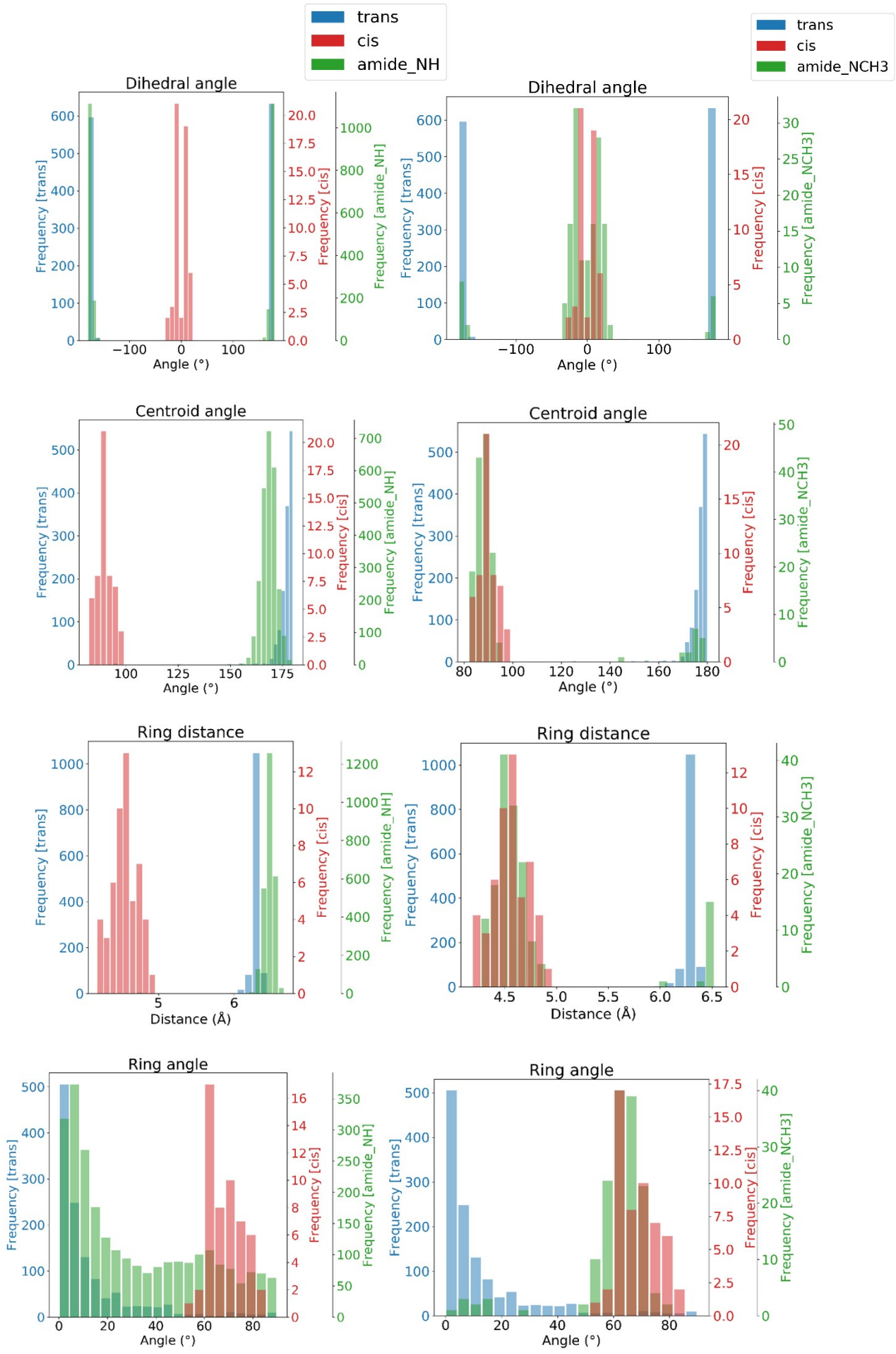

Fig. S21. Geometric distributions for *N*-unsubstitued (left, data from 2587 structures) and *N*-methylbenzanilide (right, data from 154 structures), *trans*- and *cis*-azobenzene structures in the CSD.

S4.3. Ligand search in the PDB and ChEMBL

The PDB was queried for ligands containing azobenzene and the *cisoid* substructures identified in the CSD queries. Only two ligands that featured a *cis*-azobenzene were found, which was not sufficient for any analysis.

Entry	Substructure	Hits	Comments
Azobenzene	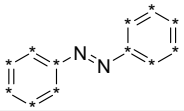	105	*Trans*-azobenzene: 103 structures.
Biaryl sulfonamide	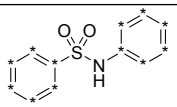	313	311 are acyclic.
N-Benzylaniline	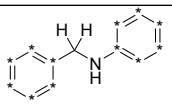	673	Both *transoid* and *cisoid.*
N-Benzyl-*N*-methylaniline	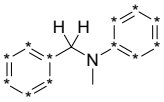	209	26 unique structures (184 out of 209 are MTX).
N-Methylbenzanilide	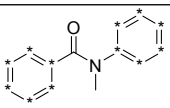	52	Only 24 structures are acyclic.

Table S2. Results of the PDB queries.

The 673 ligands with an *N*-benzylaniline showed the same tendency to adopt *transoid* and *cisoid* conformations (Fig. S22). The 221 ligands with a *N*-benzyl-*N*-methylaniline substructure mainly featured an unsubstituted carbon atom in the linker (209 hits). Moreover, 184 out of 209 hits were methotrexate (already object of azologization in previous studies),[7,8] thus the unique structures were only 26. Similarly, only 24 out of the 52 ligands with an *N*-methylbenzanilide were acyclic. On the other hand, ligands featuring a biaryl sulfonamide substructure were 311, providing many possibilities for azologization. All structures showcased a cNSc dihedral angle in the range between -100° and 100°, with no *transoid* structures. Additionally, 53 ligands were in the stricter *cisoid* range (-50° to 50°, see Fig. S23).

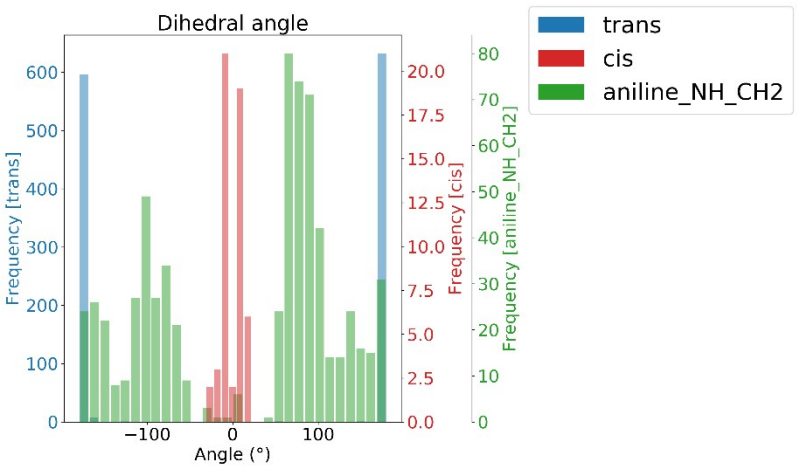

Fig. S22. Dihedral angle distributions for *N*-benzylanilines in the PDB, and *trans*- and *cis*-azobenzenes in the CSD.

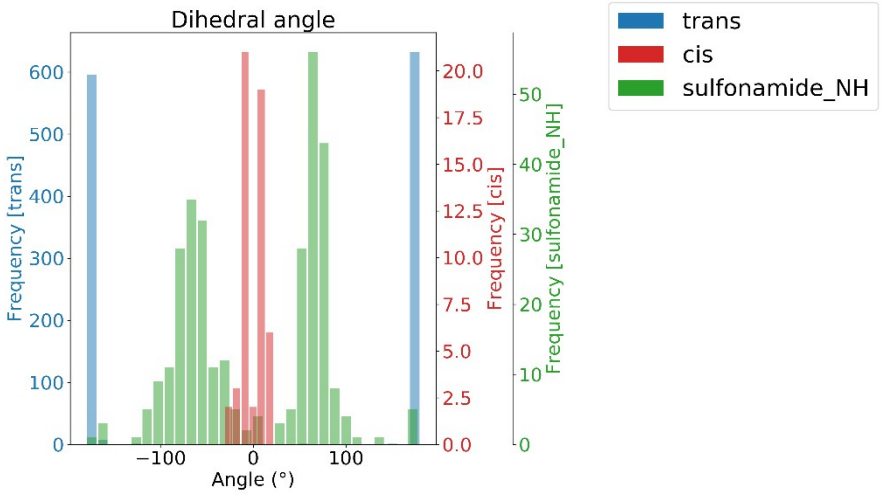

Fig. S23. Dihedral angle distributions for biaryl sulfonamides in the PDB, and *trans*- and *cis*-azobenzenes in the CSD.

Substructure	Geometry	Electronic similarity	ChEMBL hits	Useful PDB hits
Biaryl sulfonamide	*Cisoid*	Very Good	21635	311

Table S3. Overview of the selection of sulfonamides as promising *cisoid* azosteres. For considerations on electronic similarity, see Section S4.6.

S4.4. Molecular docking

The proteins were prepared through the Protein Preparation Wizard in Maestro, performing the assignment of bond orders, hydrogen addition, hydrogen bonds definition and optimization, removal of water molecules and ions, and restrained minimization with the OPLS3e force field.[9] All water molecules were removed. The grid was created through the Receptor Grid Generation. LigPrep was used to prepare the ligands and to generate possible states at pH 7.0 ± 2.0 with Epik. The ligands were docked with Induced Fit Docking XP[10,11] with standard protocol. The ligand was picked to define the centroid of the receptor box, the option "Enhance planarity of conjugated pi groups" was selected, and the side chains were trimmed based on their B-factor. The cNSc dihedral angle was constrained to the experimental value during redocking. All docking pose images were obtained with Pymol (The PyMOL Molecular Graphics System, Version 2.2.3 Schrödinger, LLC).

PDB ID: 5YEA

Measurement	Value
cNSc dihedral angle	80°
Centroid angle	103°
Ring distance	5.3 Å
Ring angle	44°

Table S4. Measurements of the ligand from PDB: 5YEA (chain B).

Chain B was selected. During redocking of the cocrystallized ligand, the cNSc dihedral angle was constrained to 80°. This resulted in a successful redocking with root-mean-square deviation (RMSD) = 1.7 Å.

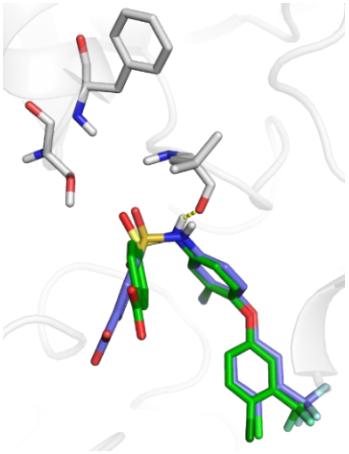

Fig. S24. Redocking of the cocrystallized ligand **Sulf-1** (PDB: 5YEA). The cocrystallized ligand is depicted in green, while the docking pose is in purple.

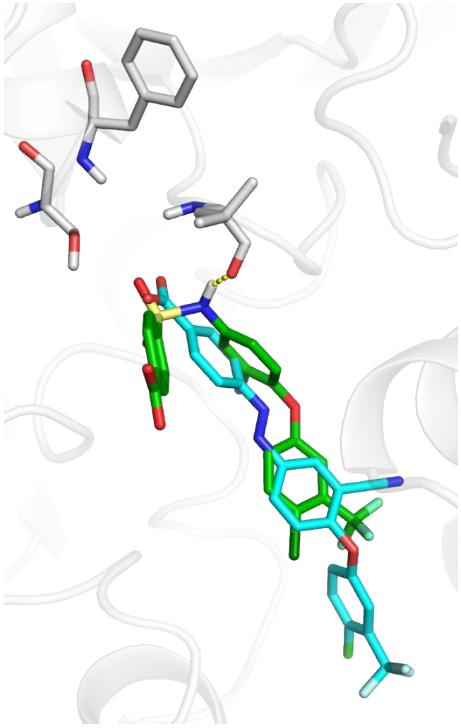

Fig. S25. Alternate docking pose of *trans*-**Azo-1** (cyan) into PDB: 5YEA, superimposed with the cocrystallized ligand **Sulf-1** (green).

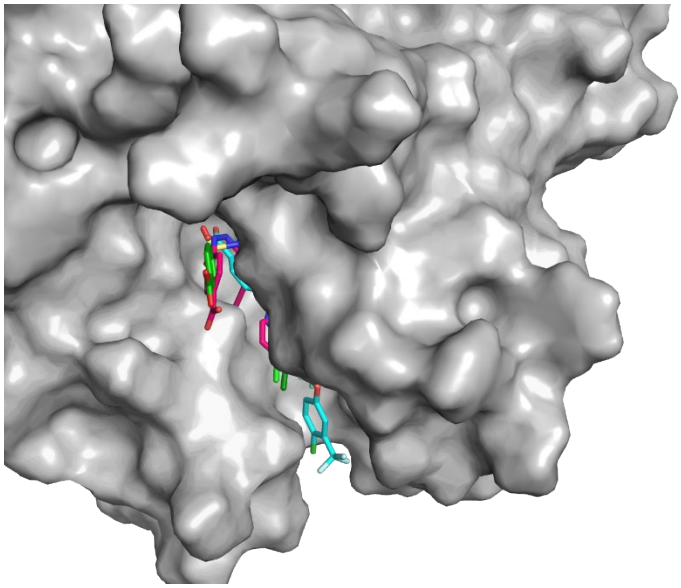

Fig. S26. Superposition of **Sulf-1** (green), *trans*-**Azo-1** (cyan) and *cis*-**Azo-1** (red). The sulfonamide is interacting deeply in the binding pocket of the protein (gray surface).

PDB ID: 5EEN and 4LXZ

Measurement	Value
cNSc dihedral angle	-60°
Centroid angle	90°
Ring distance	4.8 Å
Ring angle	68°

Table S5. Measurements of the ligand from PDB: 5EEN (chain B).

The selected ligand for azologization (belinostat, **Sulf-2**) is cocrystallized with HDAC6 (PDB: 5EEN), but HDAC2 (PDB: 4LXZ) was mainly used for modeling because of the available biological assay. To check the similarity of the enzymes, chain B was selected for both PDBs and the binding pocket residues were aligned with the Protein Structure Alignment module in Maestro. The structures showed very good alignment (RMSD = 0.94 Å, see Fig. S27) and the residues in the binding pocket are highly conserved.

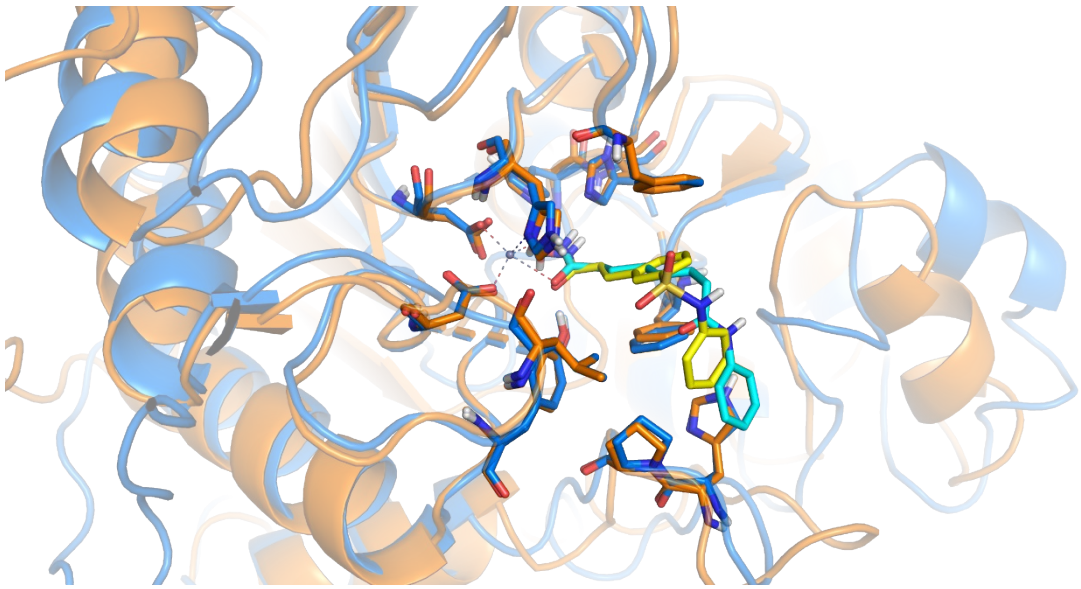

Fig. S27. Structural alignment of 4LXZ (protein in blue, ligand in cyan) and 5EEN (protein in orange, ligand in yellow).

Because of its disputed protonation state,[12,13] the hydroxamic acid was considered both in its protonated and deprotonated form. The Zn(II) and Ca(II) ions were kept during protein preparation. Also, two specific water molecules (described as WAT1 and WAT2 in a previous study[12]) were kept for 4LXZ, while they were absent in 5EEN. During the redocking of belinostat into 5EEN and the cross-docking into 4LXZ, the cNSc dihedral angle was constrained to -60°.

Entry (Fig.)	RMSD (Å)
4LXZ protonated (S26)	1.1
4LXZ deprotonated (S27)	1.6
5EEN protonated (S28)	2.7
5EEN deprotonated (S29)	2.6
Cross-docking of **Sulf-2** in 4LXZ protonated (S30)	2.7
Cross-docking of **Sulf-2** in 4LXZ deprotonated (S31)	3.2

Table S6. RMSDs for the redocking and cross-docking experiments.

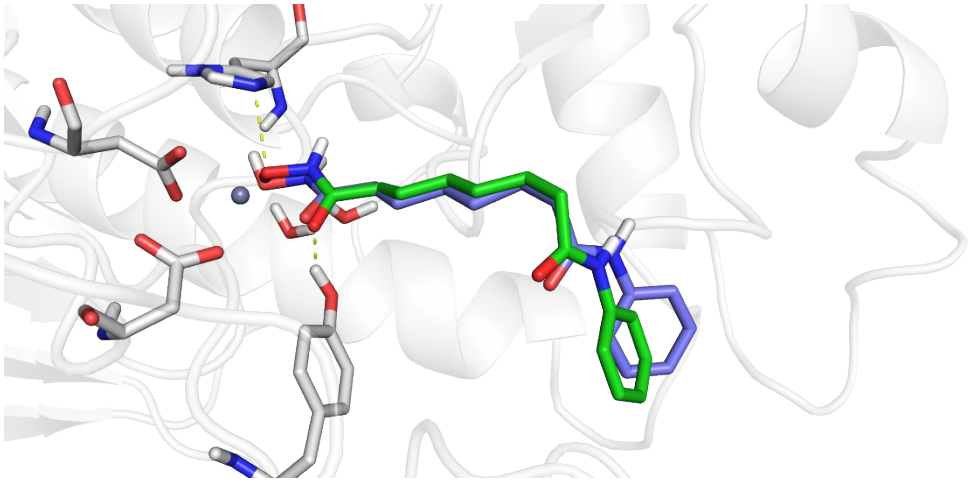

Fig. S28. Redocking of the protonated cocrystallized ligand (PDB: 4LXZ). The cocrystallized ligand is depicted in green, while the docking pose is in purple.

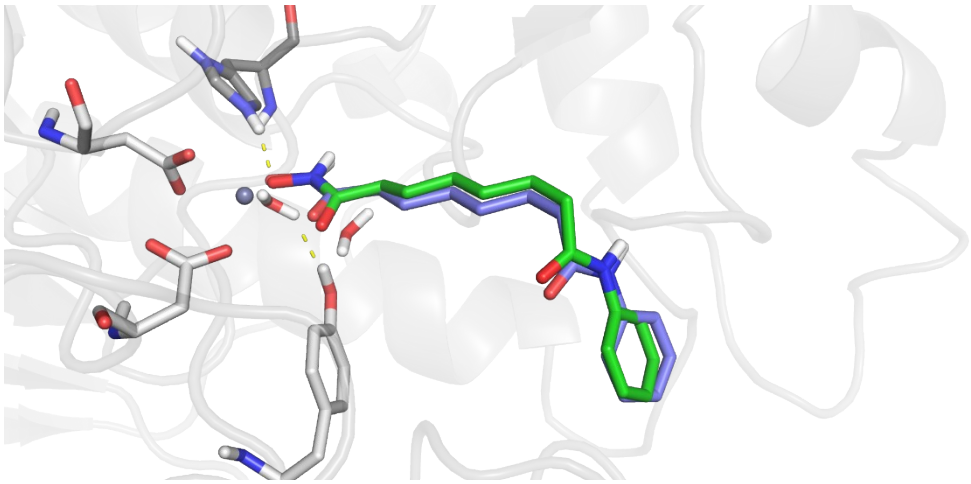

Fig. S29. Redocking of the deprotonated cocrystallized ligand (PDB: 4LXZ). The cocrystallized ligand is depicted in green, while the docking pose is in purple.

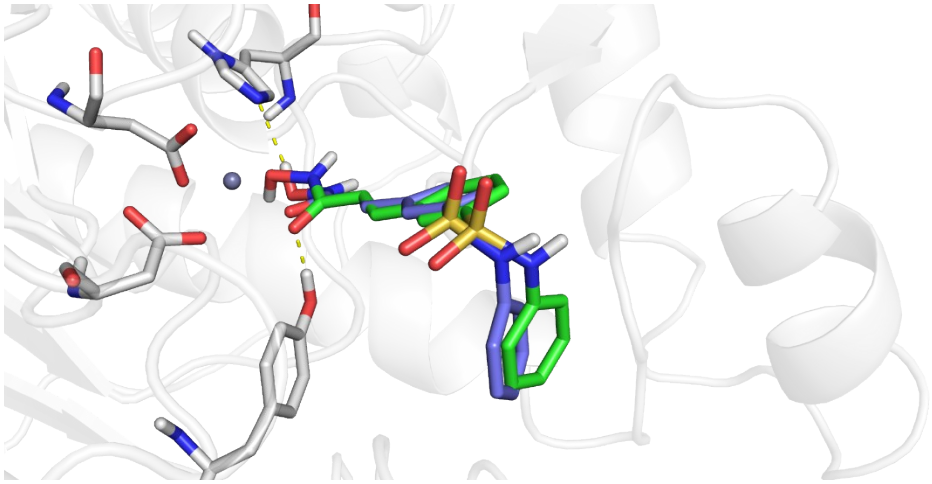

Fig. S30. Redocking of the protonated cocrystallized ligand (PDB: 5EEN). The cocrystallized ligand is depicted in green, while the docking pose is in purple.

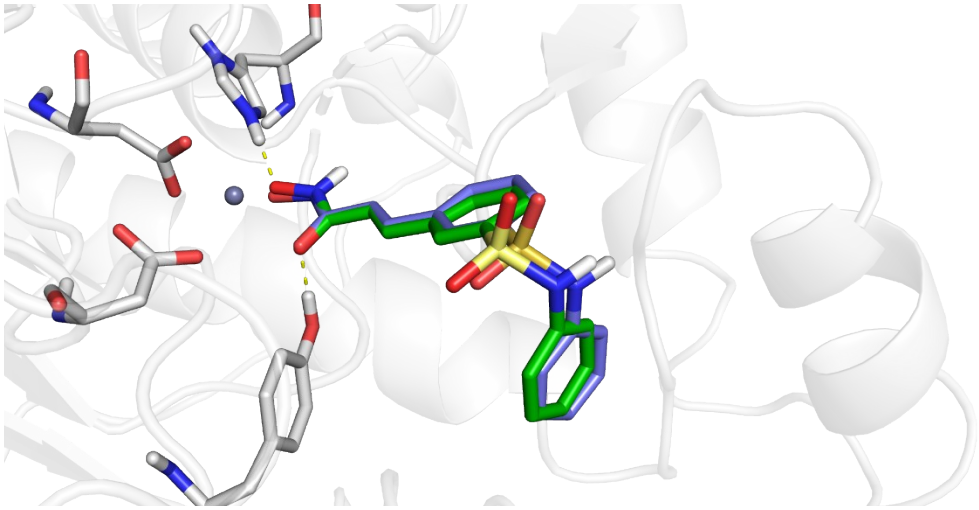

Fig. S31. Redocking of the deprotonated cocrystallized ligand (PDB: 5EEN). The cocrystallized ligand is depicted in green, while the docking pose is in purple.

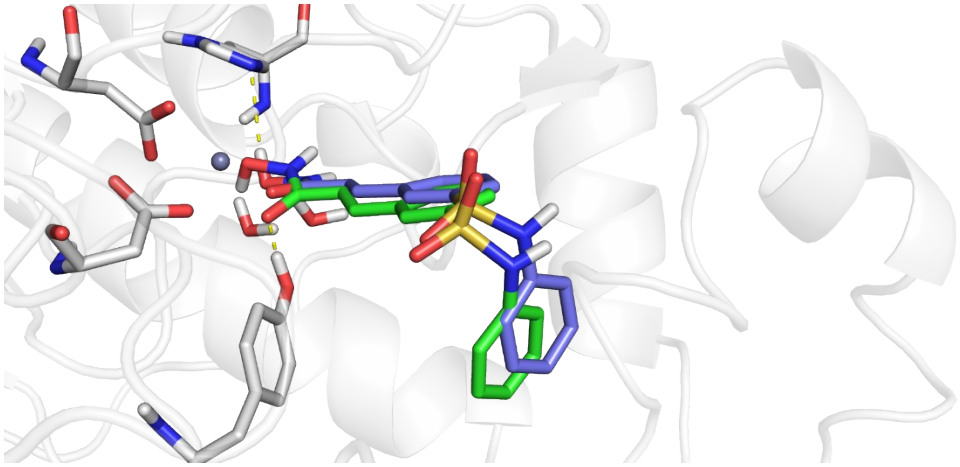

Fig. S32. Cross-docking of protonated **Sulf-2** into PDB: 4XLZ. The ligand from PDB: 5EEN is depicted in green, while the docking pose is in purple.

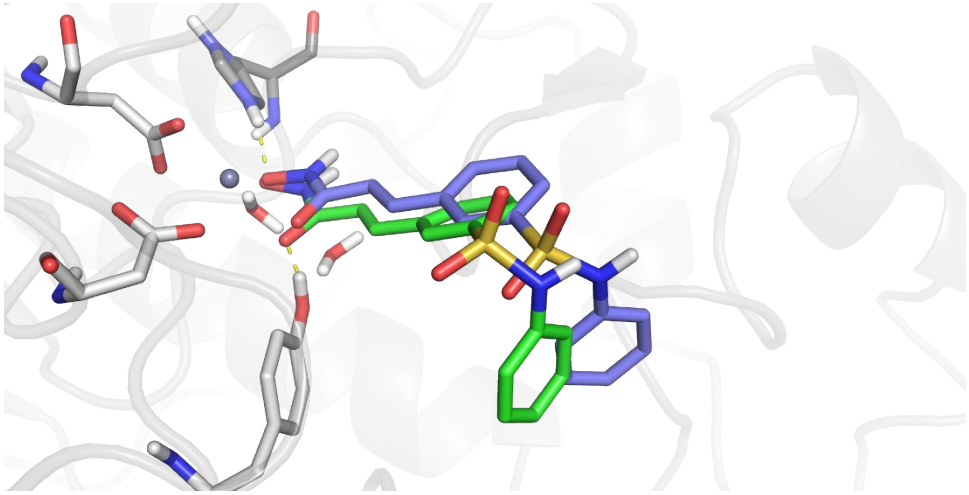

Fig. S33. Cross-docking of deprotonated **Sulf-2** into PDB: 4XLZ. The ligand from PDB: 5EEN is depicted in green, while the docking pose is in purple.

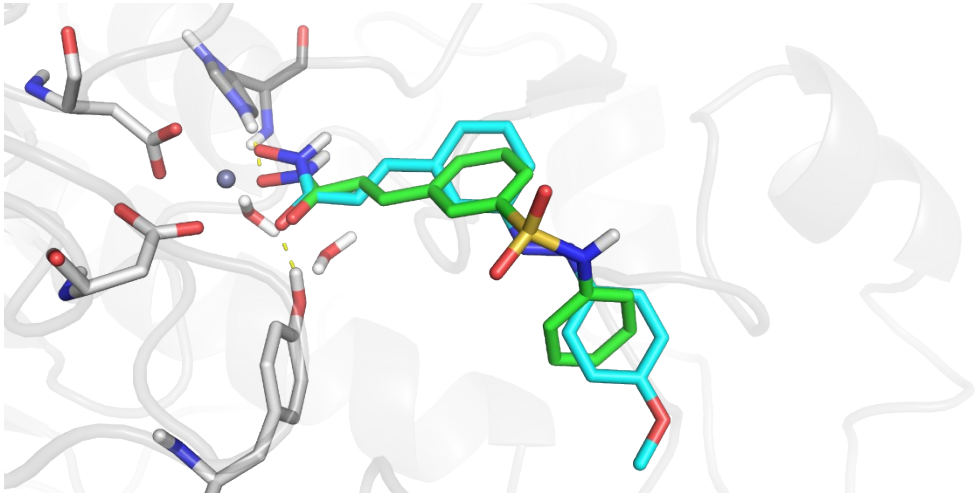

Fig. S34. Docking pose of deprotonated *trans*-**Azo-2** (cyan) into PDB: 4XLZ, superimposed with the docking pose of belinostat (green).

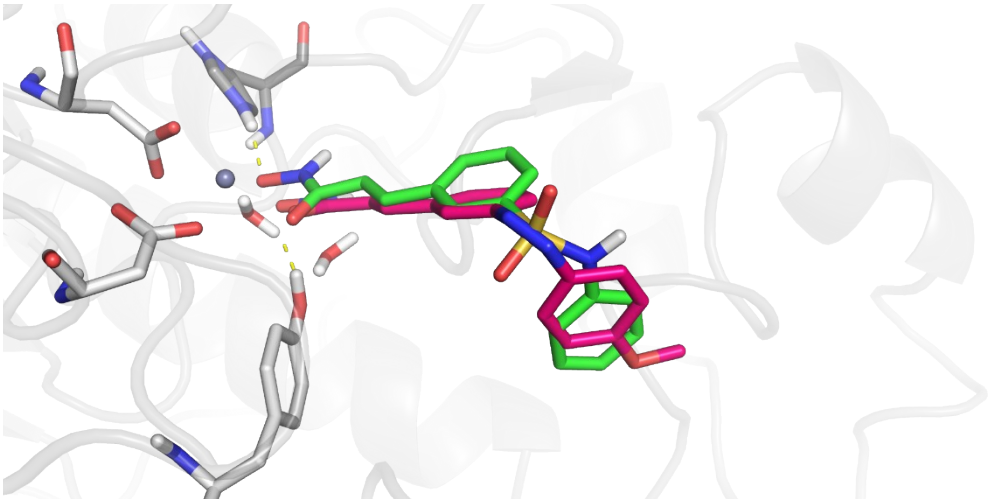

Fig. S35. Docking pose of deprotonated *cis*-**Azo-2** (red) into PDB: 4XLZ, superimposed with the docking pose of belinostat (green).

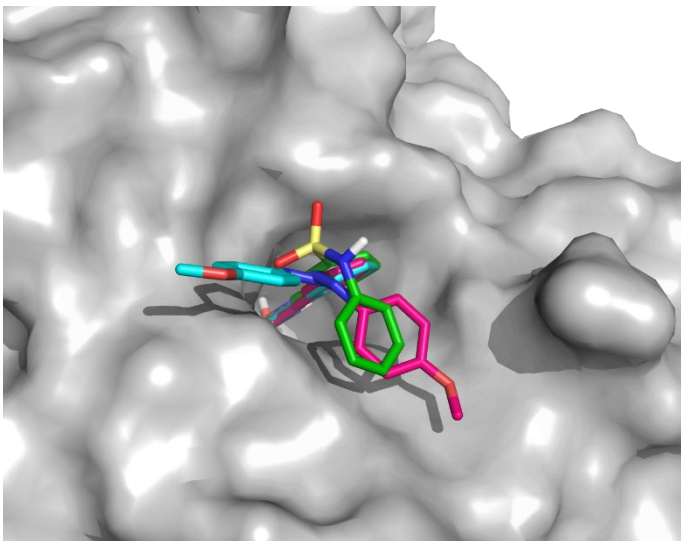

Fig. S36. Docking poses of protonated **Sulf-2** (green) and *cis*-**Azo-2** (red) show a favorable fit with the protein surface (gray), as compared to *trans*-**Azo-2** (cyan).

S4.5. Molecular dynamics simulations

The crystal or docking structures were embedded in a orthorhombic box of circa 11,000 TIP3P[14] water molecules with 0.1 M NaCl, and the dimension of the box was circa 100x100x100 Å. The net charge of the system was neutralized by addition of sodium ions to the solvent box. The total number of atoms was circa 40,000 atoms. The simulations were performed with the Desmond molecular dynamics package,[15] with default settings for bond-constrains, Van der Waals and electrostatic interactions cutoffs, and PME method[16] for long range electrostatic interactions.

Each system was subjected to the following relaxation and equilibration protocol: 100 ps of Brownian dynamics at 10 K in an NVT ensemble with harmonic restraints (50 kcal/mol/A^2) on the solutes heavy atoms, followed by 12 ps in an NVT ensemble (Berendsen thermostat)[17] at 10 K and retaining harmonic restraints on the solutes heavy atoms, followed by 12 ps in an NPT ensemble (Berendsen thermostat and barostat) at 10 K and retaining harmonic restraints on the solutes heavy atoms, followed by 24 ps in an NPT ensemble (Berendsen thermostat and barostat) at 300 K and retaining harmonic restraints on the solutes heavy atoms, followed by 24 ps in an NPT ensemble (Berendsen thermostat and barostat) at 300 K without harmonic restraints on the solutes heavy atoms. The production simulations were run for 100 ns in an NPT ensemble (300 K, 1 bar, Martyna-Tobias-Klein barostat and Nose-Hoover thermostat),[18,19] in three replicas.[20] Coordinates were saved every 100 ps and analyzed in Maestro to yield the RMSD of the ligand heavy atoms after least square fitting to the protein heavy atoms.

PDB ID: 5YEA

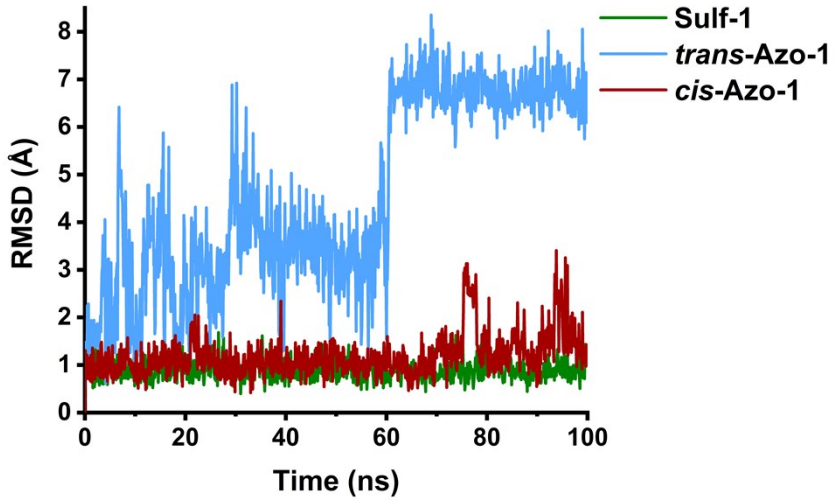

Fig. S37. RMSD of ligands throughout the second replica of 100 ns MD simulations.

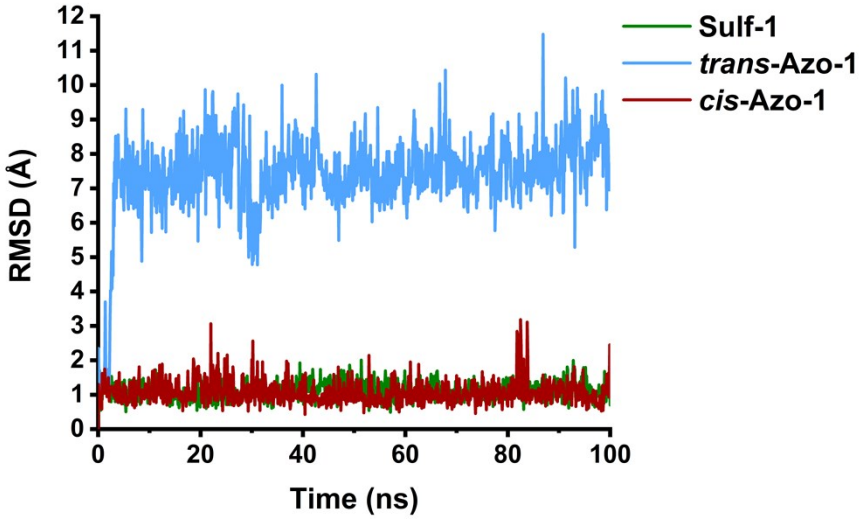

Fig. S38. RMSD of ligands throughout the third replica of 100 ns MD simulations.

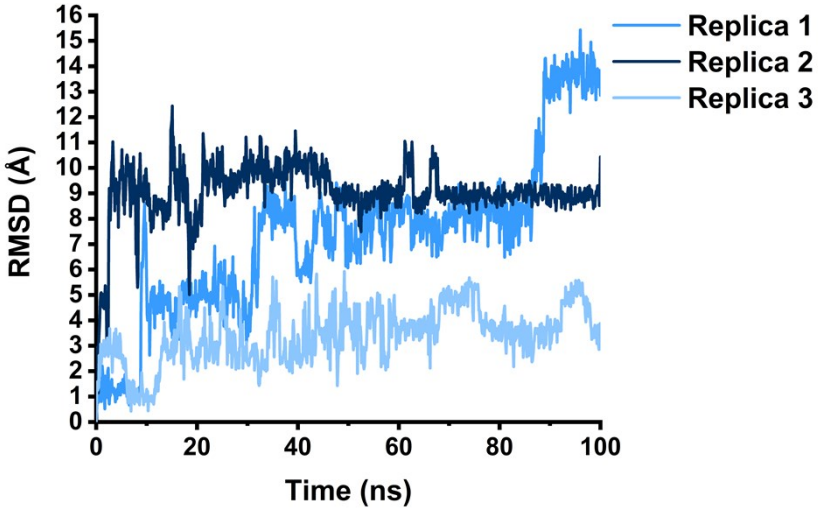

Fig. S39. RMSD of *trans*-**Azo-1** throughout three replicas of 100 ns MD simulations, starting from the alternate docking pose (see Fig. S23).

PDB ID: 4LXZ and 5EEN

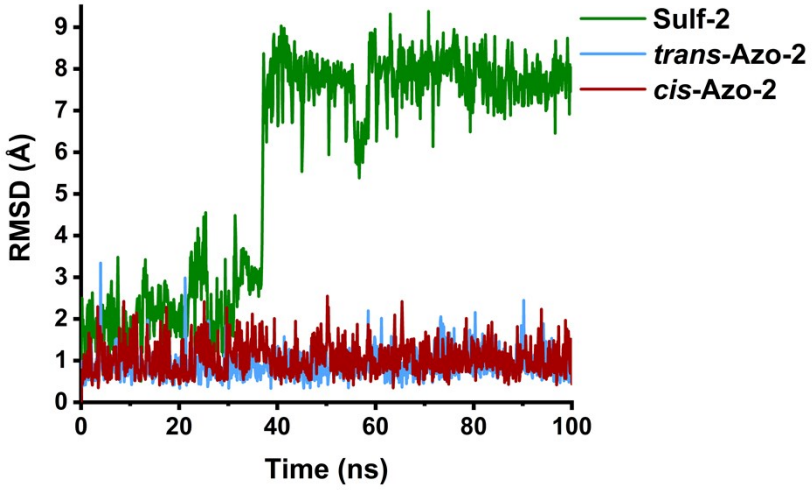

Fig. S40. RMSD of ligands throughout the second replica of 100 ns MD simulations with protonated hydroxamic acid.

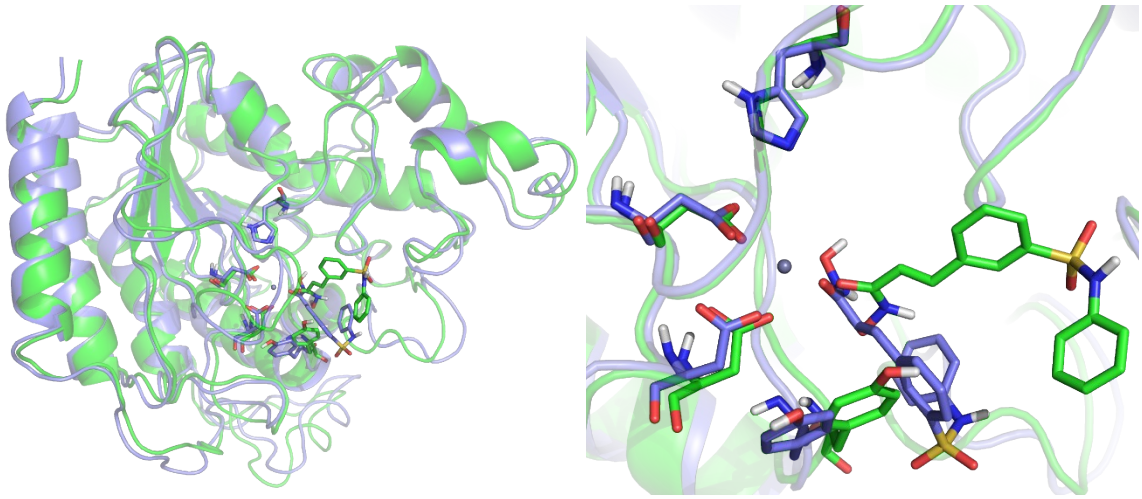

Fig. S41. Superposition of two snapshots from the previous MD run, taken at frame 1 (0 ns, green) and frame 865 (86.4 ns, purple).

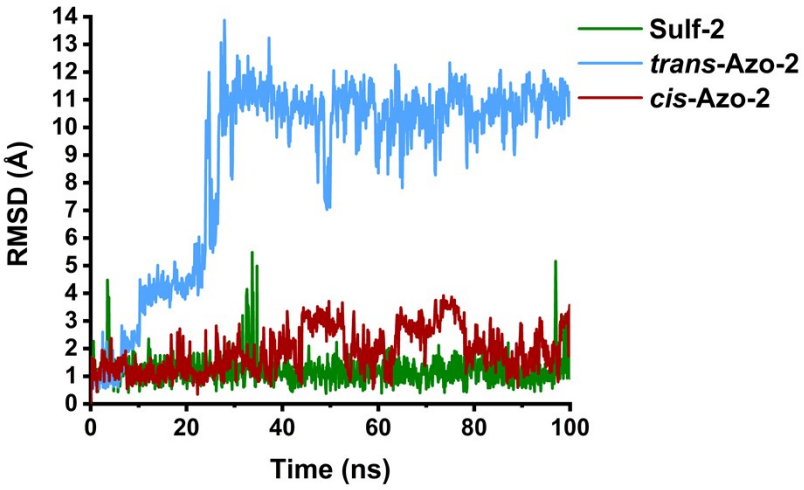

Fig. S42. RMSD of ligands throughout the third replica of 100 ns MD simulations with protonated hydroxamic acid.

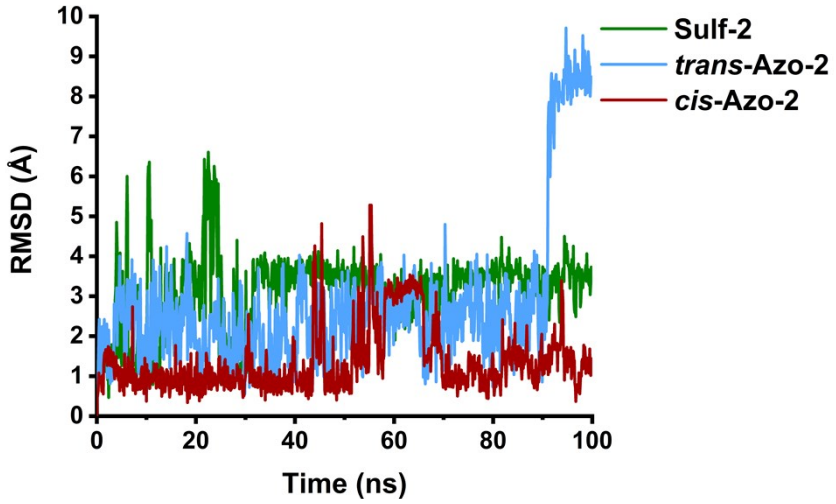

Fig. S43. RMSD of ligands throughout the first replica of 100 ns MD simulations with deprotonated hydroxamic acid.

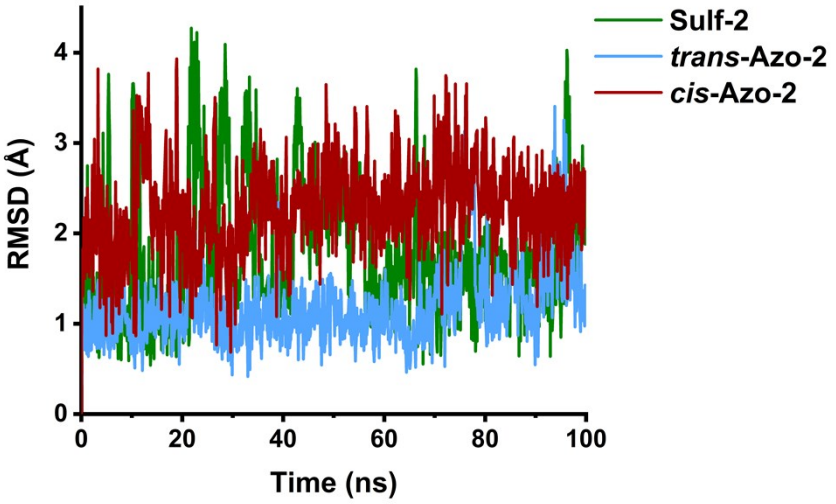

Fig. S44. RMSD of ligands throughout the second replica of 100 ns MD simulations with deprotonated hydroxamic acid.

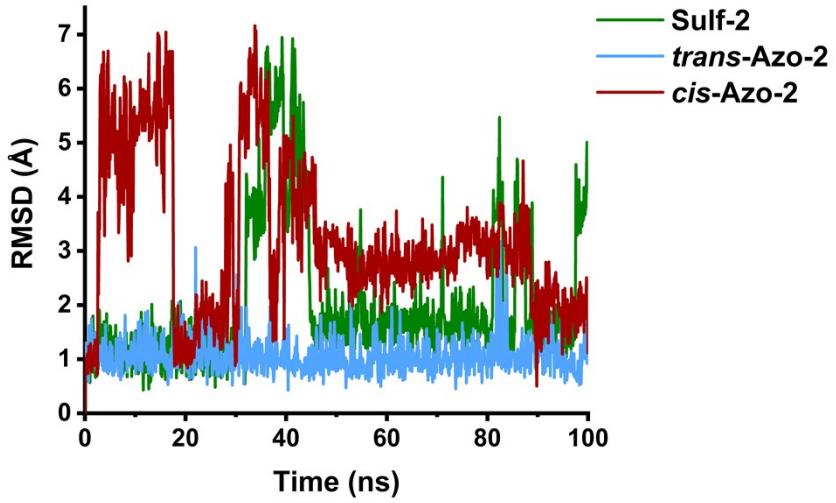

Fig. S45. RMSD of ligands throughout the third replica of 100 ns MD simulations with deprotonated hydroxamic acid.

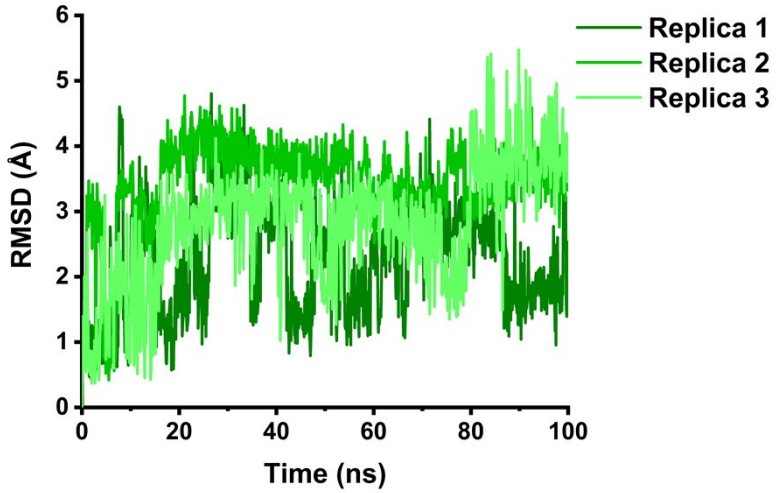

Fig. S46. RMSD of protonated **Sulf-2** throughout three replicas of 100 ns MD simulations, starting from PDB: 5EEN.

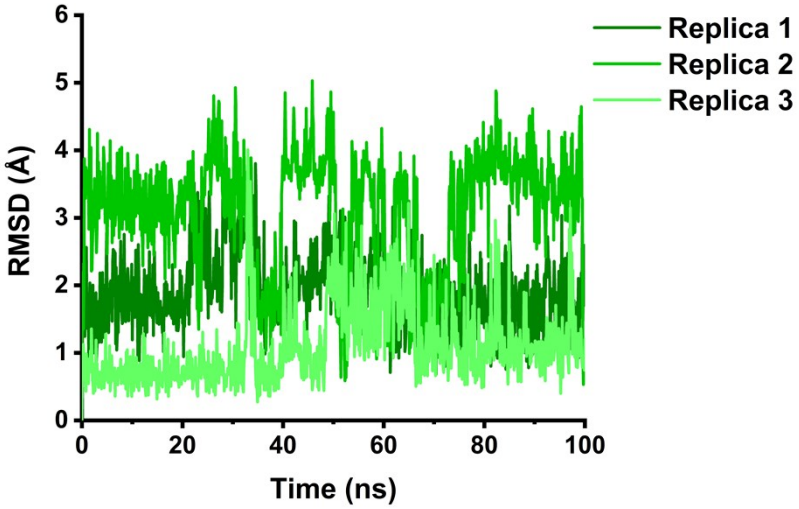

Fig. S47. RMSD of deprotonated **Sulf-2** throughout three replicas of 100 ns MD simulations, starting from PDB: 5EEN.

S4.6. Density Functional Theory (DFT) calculations

The models were constructed using the software Maestro. Geometries were initially optimized with MacroModel (Force Field: OPLS3e, vacuum, Method: PRCG). Afterwards, the geometries were further optimized with Jaguar[21] at the M06-2X-D3/6-311G++(d,p) level, in vacuo and in a CPCM water model with Bondi radius, with accuracy level: Ultrafine (in vacuo) or Fully analytics (in water), SCF convergence criteria: energy change of $1x10^{-6}$ hartree and RMS density matrix change of $1x10^{-7}$ hartrees, tight convergence criteria (iaccg=5 in the input file) and the option "Switch to analytic integrals near convergence" on (off in water). Single point energies were calculated at the same level of theory and with the same options. Frequency analysis showed zero imaginary frequencies for all the optimized structures. Electrostatic potential surfaces of the fragments were generated by mapping the electrostatic potentials onto surfaces of molecular electron density (0.001 electron/Å) and rainbow color-coding. The potential energy values range from +30 kcal/mol to -36 kcal/mol, where red color represents maximum negative potential and violet color represents maximum positive potential. Dipole moments were calculated at the M06-2X-D3/aug-cc-pVTZ(-f) level of theory (same convergence criteria, but accuracy level: Fully analytic).

Fragments

A

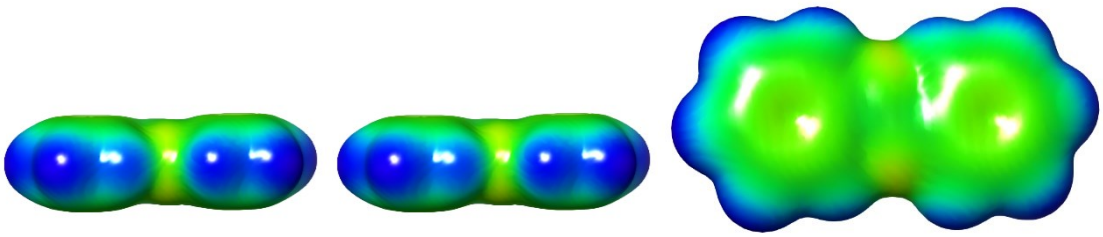

B

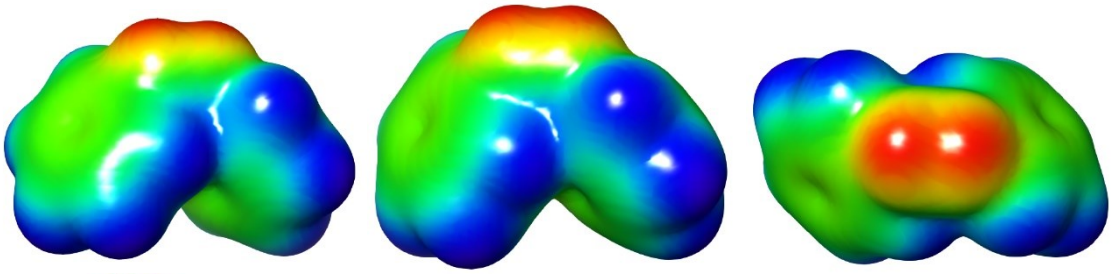

C

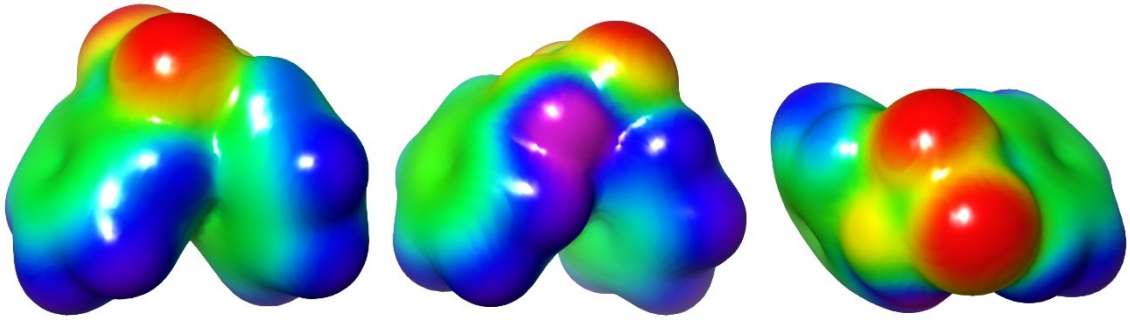

D

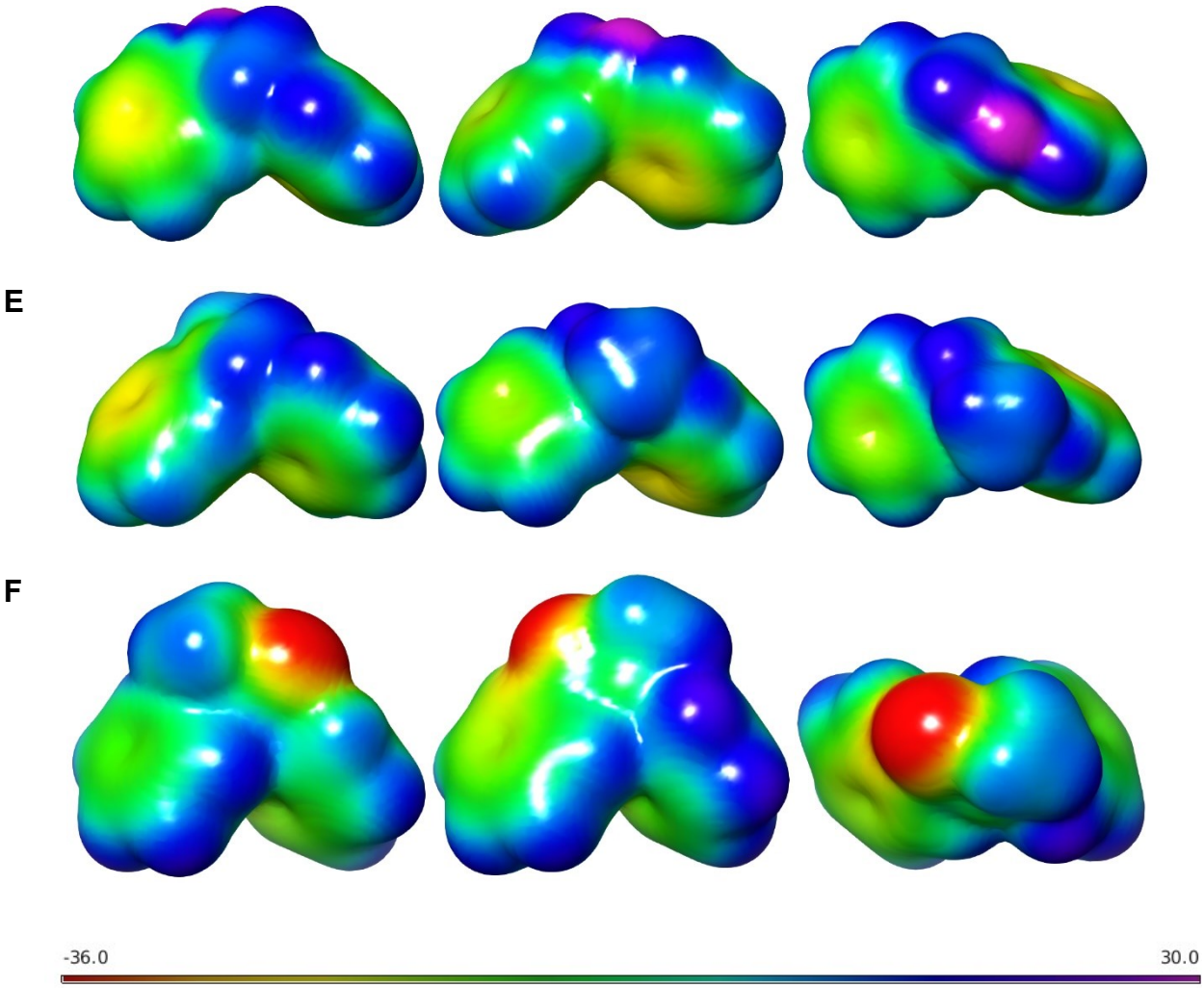

Fig. S48. Electrostatic potential (ESP) surfaces for (A) *trans*-, (B) *cis*-azobenzene and the fragments identified as *cisoid*: (C) biaryl sulfonamide, (D) *N*-benzylaniline, (E) *N*-benzyl-*N*-methylaniline, (F) *N*-methylbenzanilide. From negative to positive ESP values: red, yellow, green, blue, violet.

Ligand	μ (D) vacuum	μ (D) water
trans-Azobenzene	0	0
cis-Azobenzene	3.3	4.5
Biaryl sulfonamide	5.8	8.5
N-Benzylaniline	1.5	2.4
N-Benzyl-*N*-methylaniline	1.6	2.8
N-Methylbenzanilide	3.6	5.4

Table S7. Dipole moments calculated at the M06-2X-D3/aug-CC-PVTZ(-F) level of theory, in vacuum and in a CPCM water model.

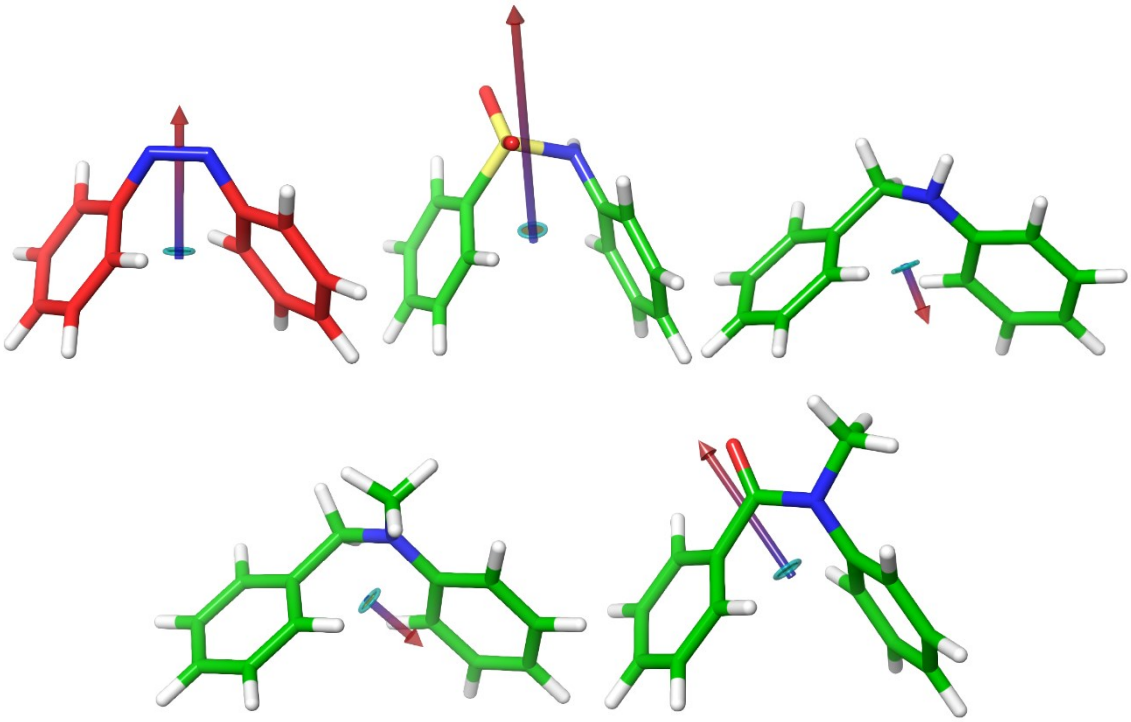

Fig. S49. Dipole moment vectors for (from left to right) *cis*-azobenzene and the fragments identified as *cisoid*: biaryl sulfonamide, *N*-benzylaniline, *N*-benzyl-*N*-methylaniline, *N*-methylbenzanilide.

Ligands

All the ionizable groups (carboxylic and hydroxamic acids) were kept in their protonated states.

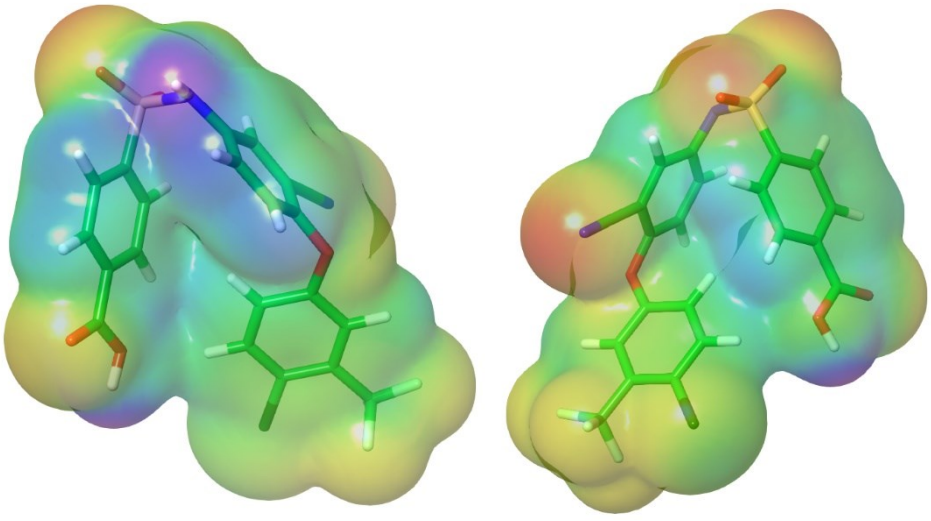

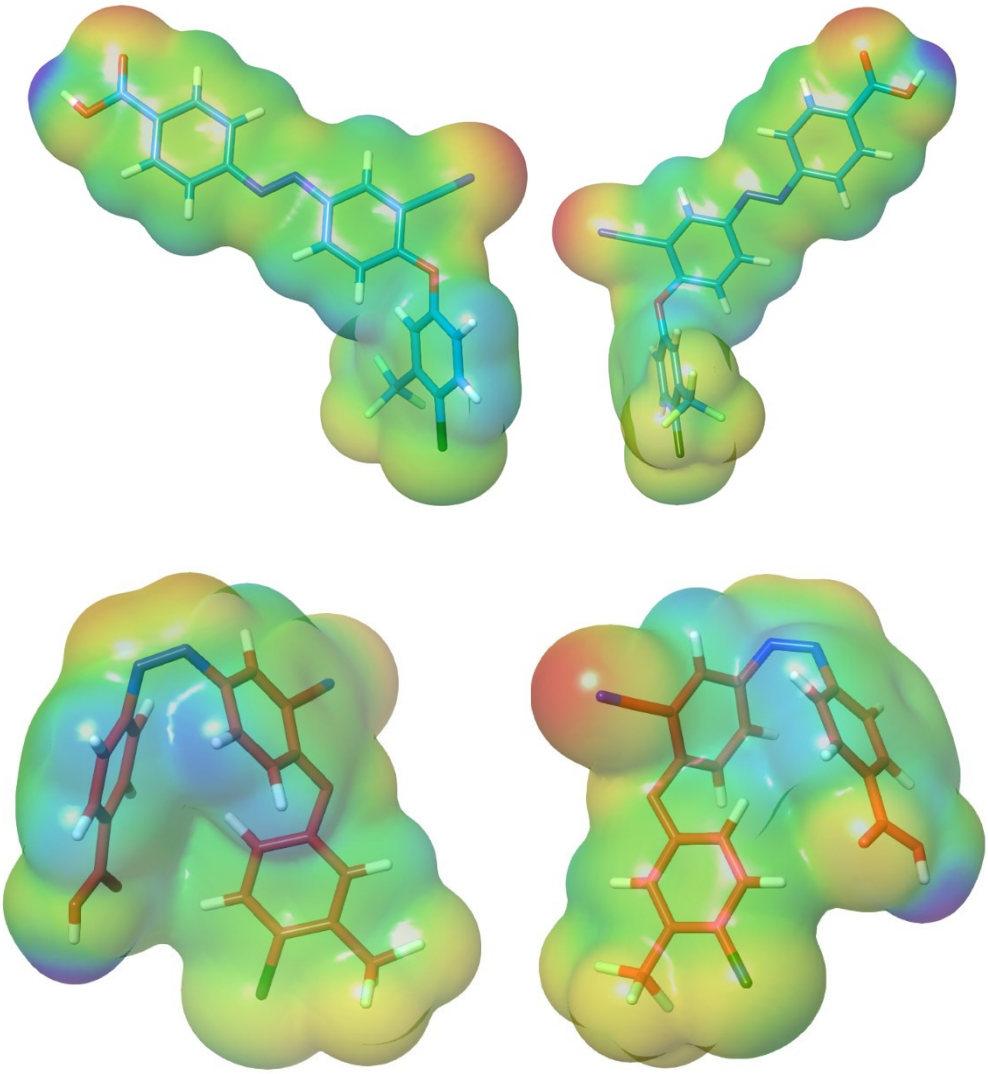

Fig. S50. Electrostatic potential (ESP) surfaces for (from top to bottom) **Sulf-1**, *trans*-**Azo-1**, and *cis*-**Azo-1**. From negative to positive ESP values: red, yellow, green, blue, violet.

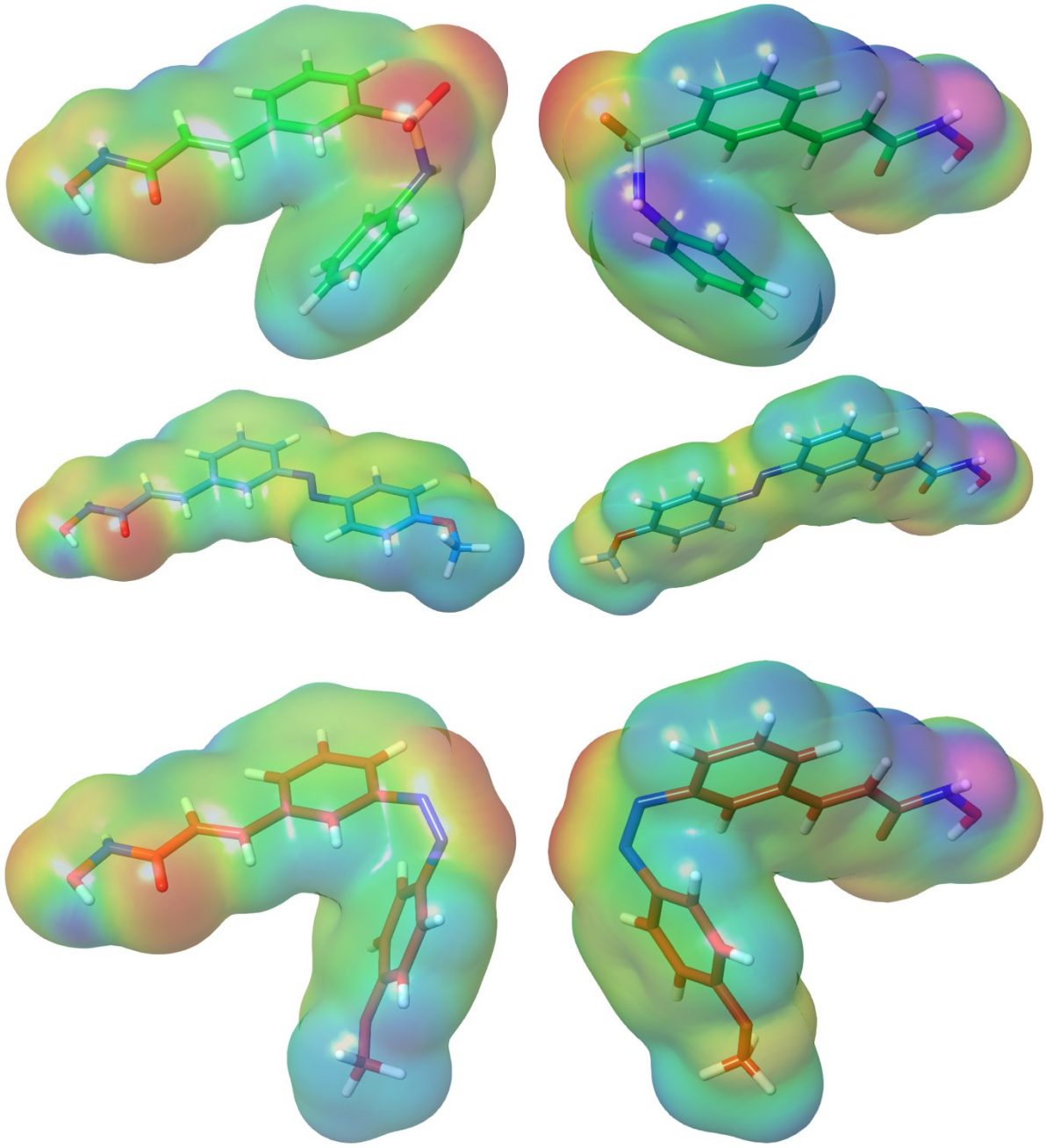

Fig. S51. Electrostatic potential (ESP) surfaces for (from top to bottom) **Sulf-2**, *trans*-**Azo-2**, and *cis*-**Azo-2**. From negative to positive ESP values: red, yellow, green, blue, violet.

Ligand	μ (D) vacuum	μ (D) water
Sulf-1	6.4	9.1
trans-Azo-1	5.1	7.0
cis-Azo-1	6.6	7.8

Table S8. Dipole moments of the Lp-PLA_2 ligands, calculated at the M06-2X-D3/aug-CC-PVTZ(-F) level of theory in vacuum and in a CPCM water model.

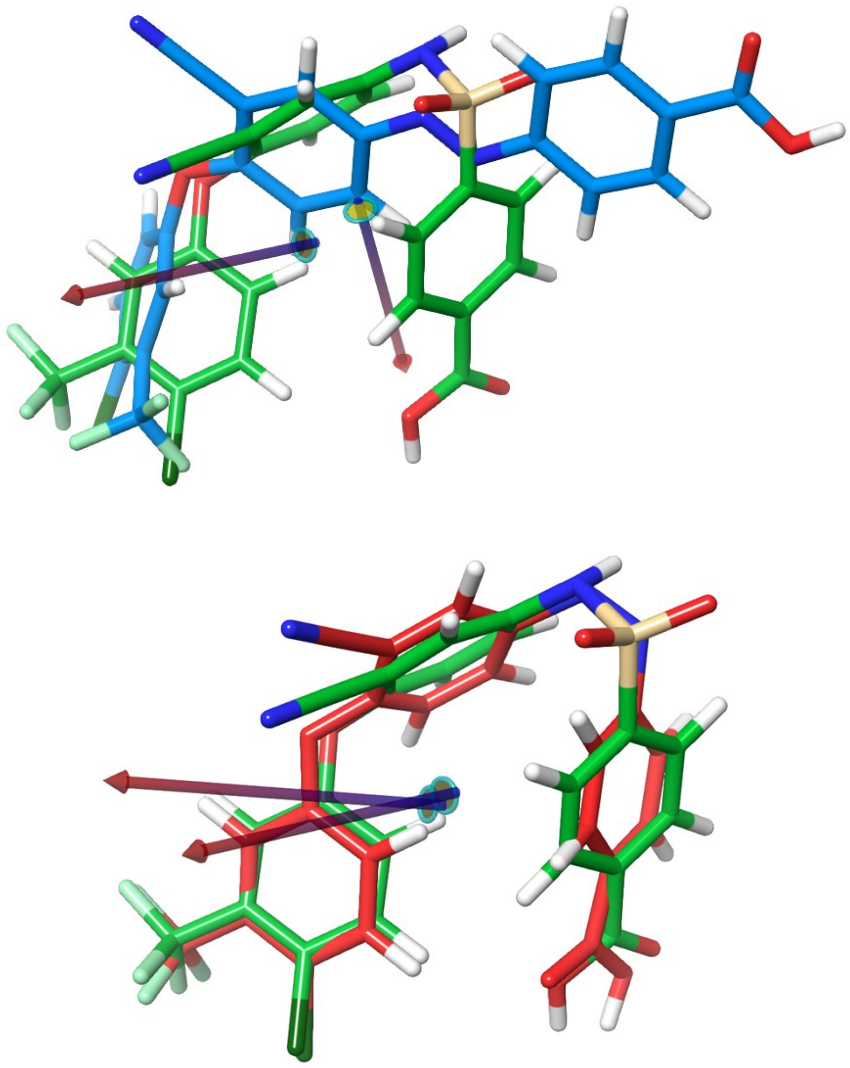

Fig. S52. (top) Dipole moment vectors for *trans*-**Azo-1** (cyan) superimposed on **Sulf-1** (green). (bottom) Dipole moment vectors for *cis*-**Azo-1** (red) superimposed **Sulf-1** (green).

Ligand	μ (D) vacuum	μ (D) water
Sulf-2	6.3	10.4
trans-Azo-2	3.4	3.2
cis-Azo-2	3.4	5.0

Table S9. Dipole moments of the HDAC2 ligands, calculated at the M06-2X-D3/aug-CC-PVTZ(-F) level of theory in vacuum and in a CPCM water model.

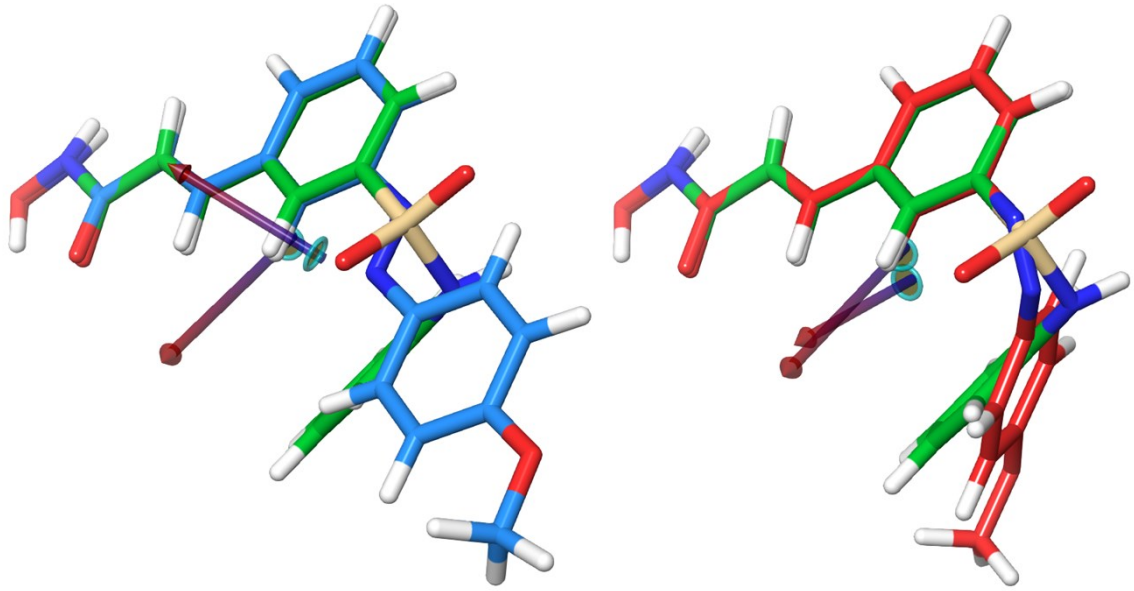

Fig. S53. (left) Dipole moment vectors for *trans*-**Azo-2** (cyan) superimposed on **Sulf-2** (green). (right) Dipole moment vectors for *cis*-**Azo-2** (red) superimposed **Sulf-2** (green).

S5. NMR and HRMS Data

Compound S1 (^{1}H-NMR, 400 MHz, DMSO-d_6)

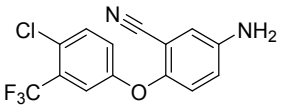

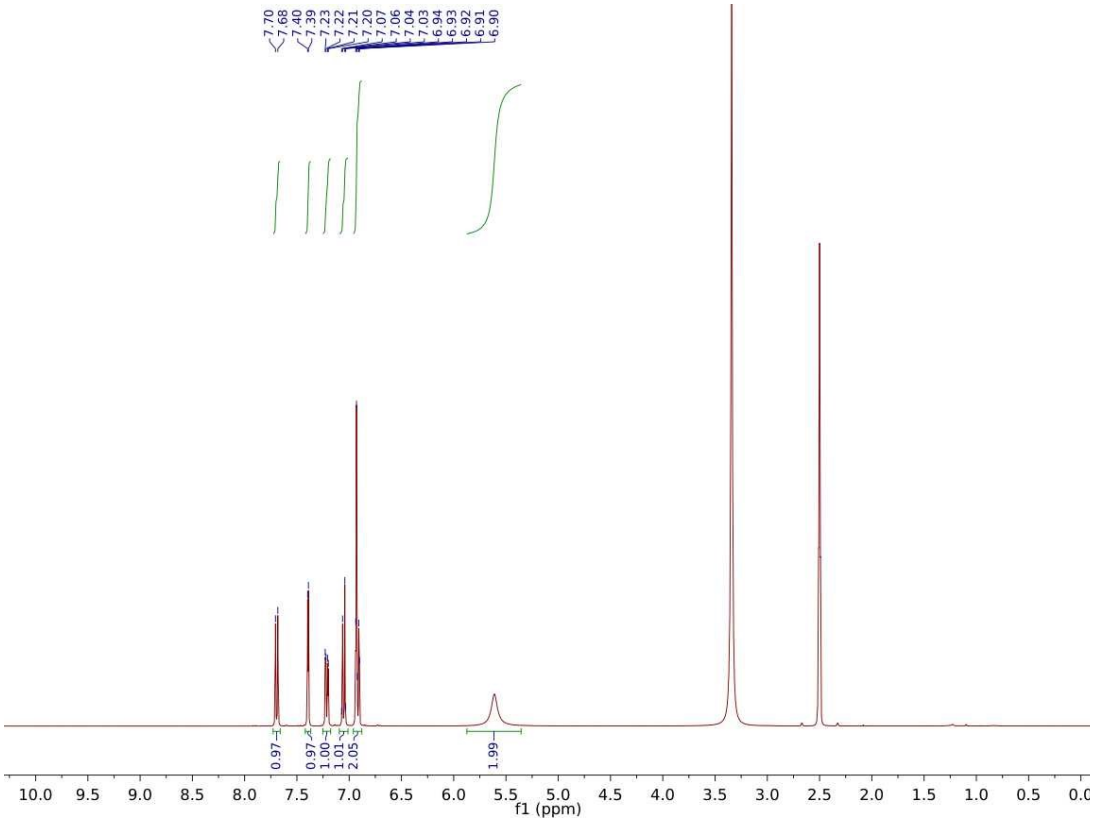

Compound S1 (HRMS)

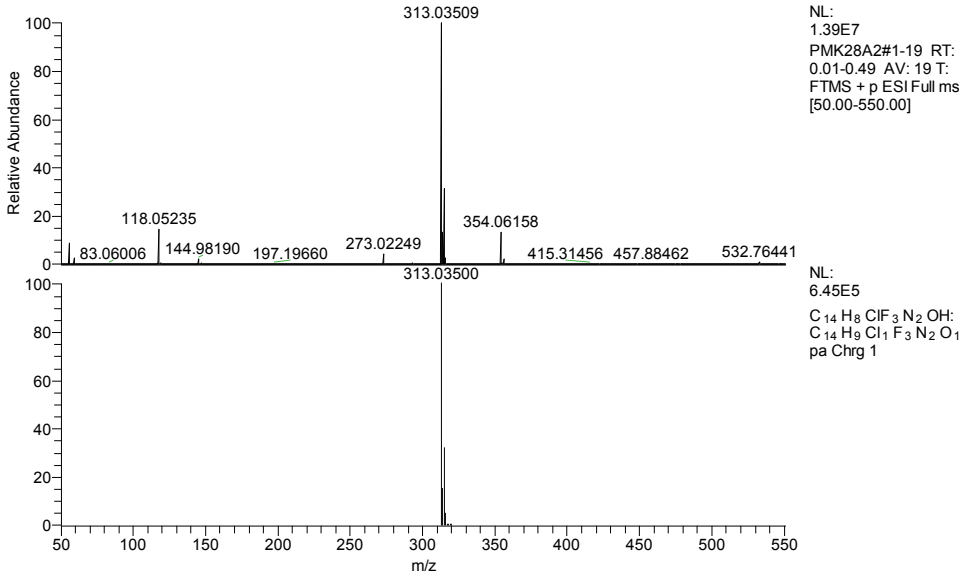

Compound Sulfo-1 (^{1}H-NMR, 400 MHz, DMSO-d_6)

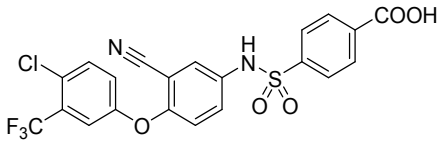

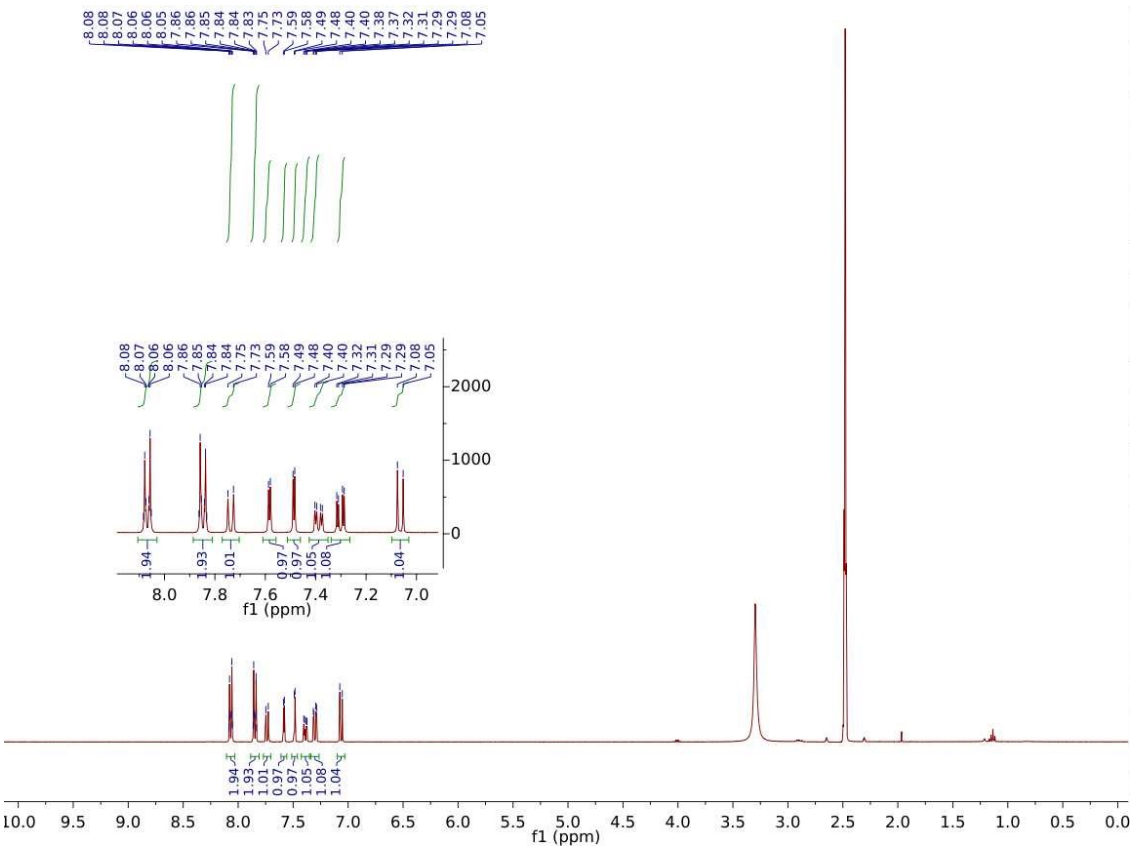

Compound Sulfo-1 (HRMS)

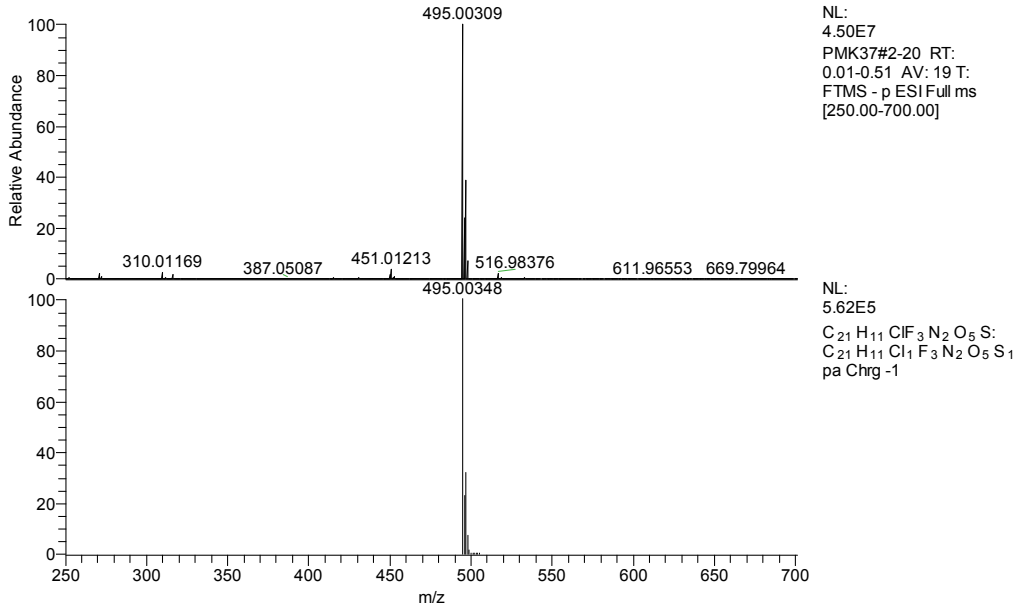

Compound Azo-1 (^{1}H-NMR, 400 MHz, DMSO-d_6)

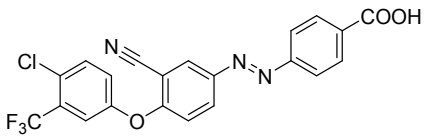

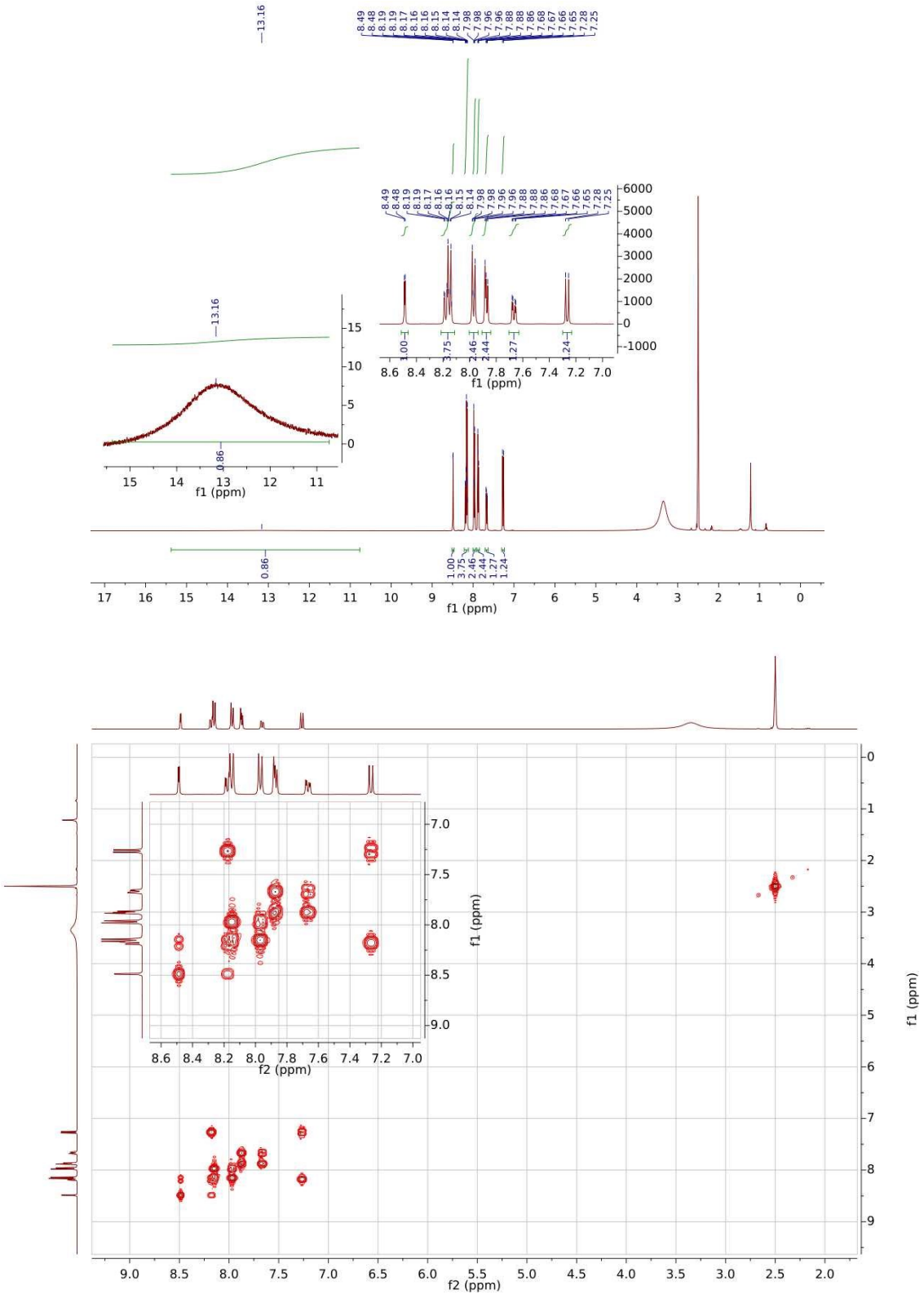

Compound Azo-1 (^{13}C-NMR, 101 MHz, DMSO-d_6)

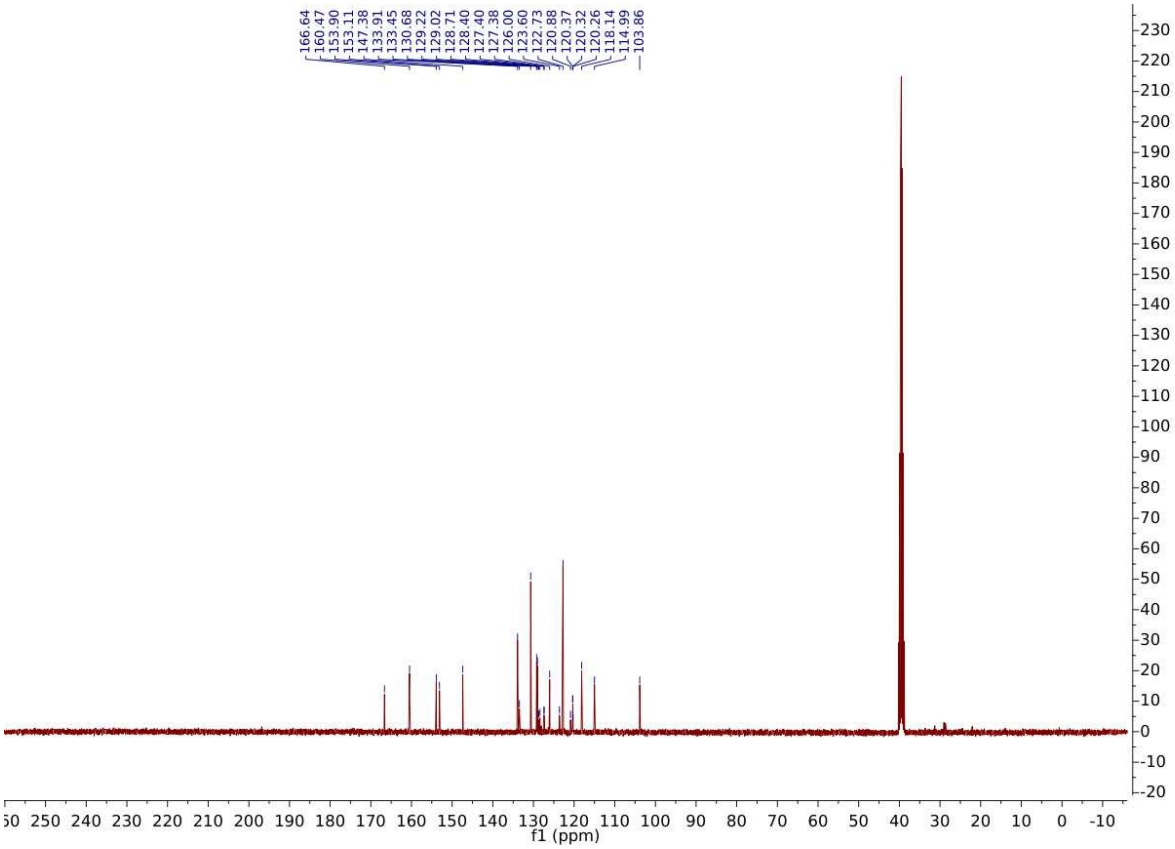

Compound Azo-1 (HRMS)

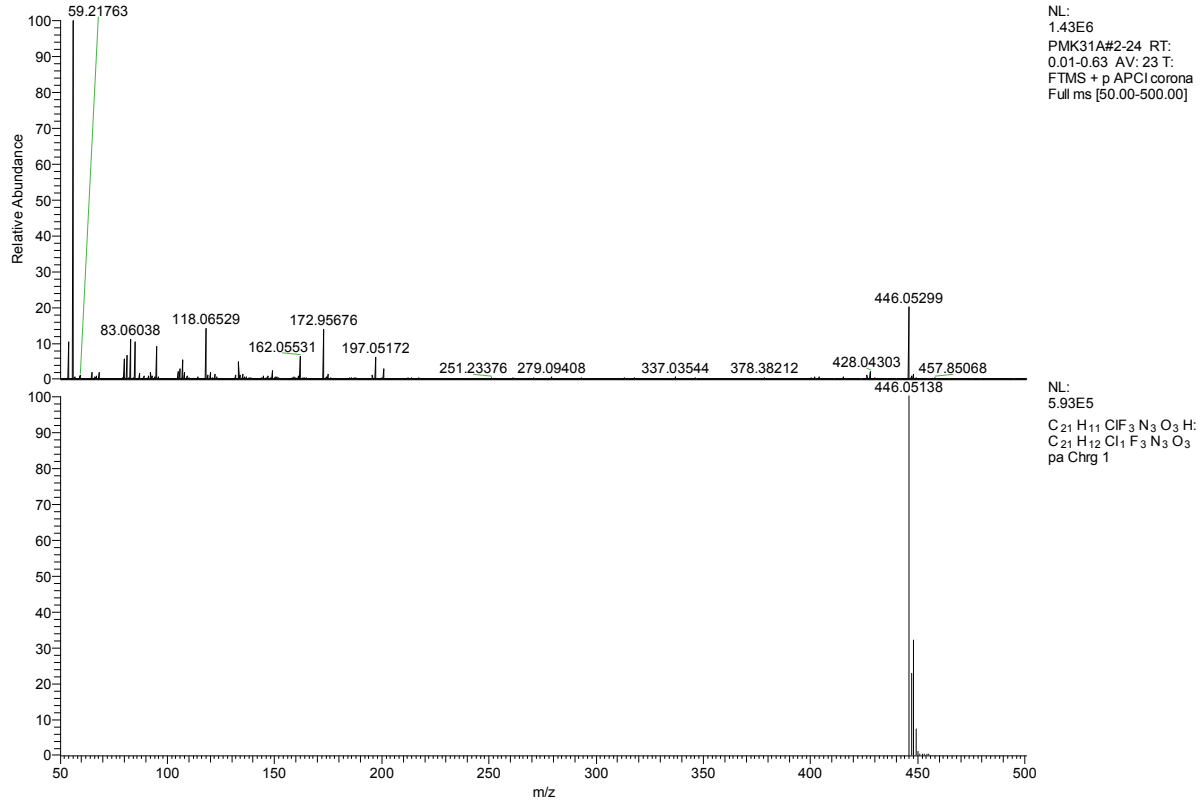

Compound S4 (^{1}H-NMR, 400 MHz, $CDCl_3$)

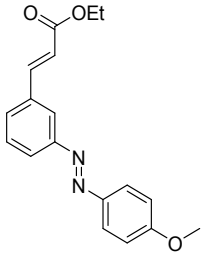

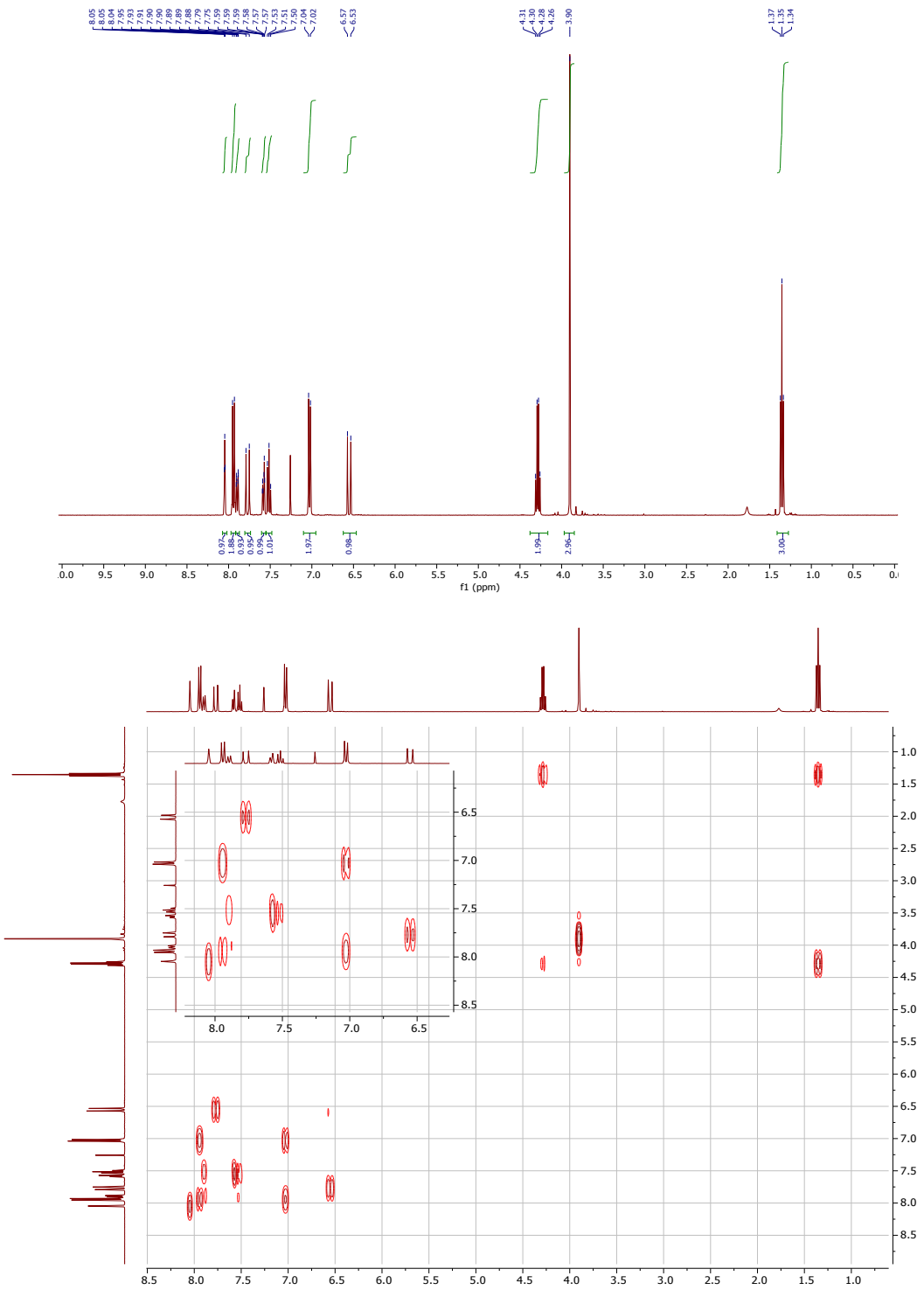

Compound S4 (^{13}C-NMR, 101 MHz, $CDCl_3$)

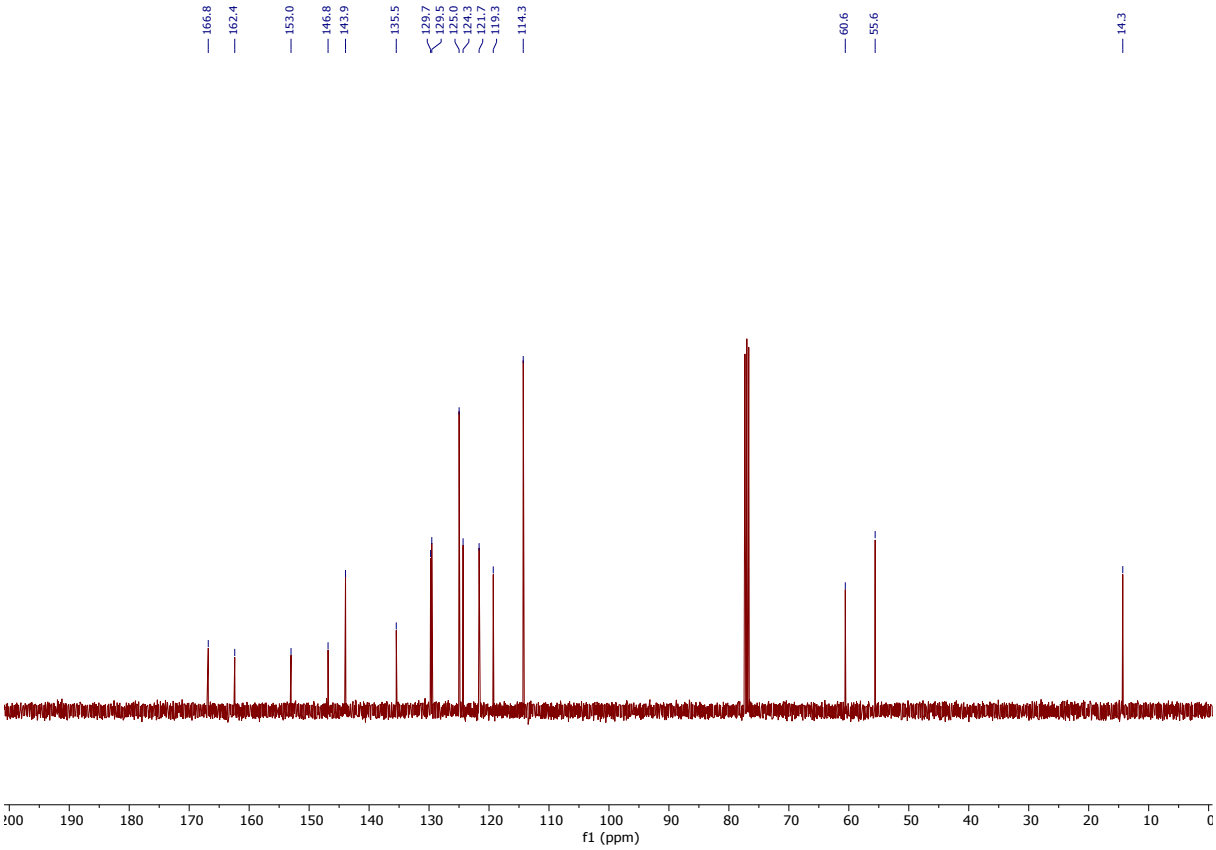

Compound S4 (HRMS)

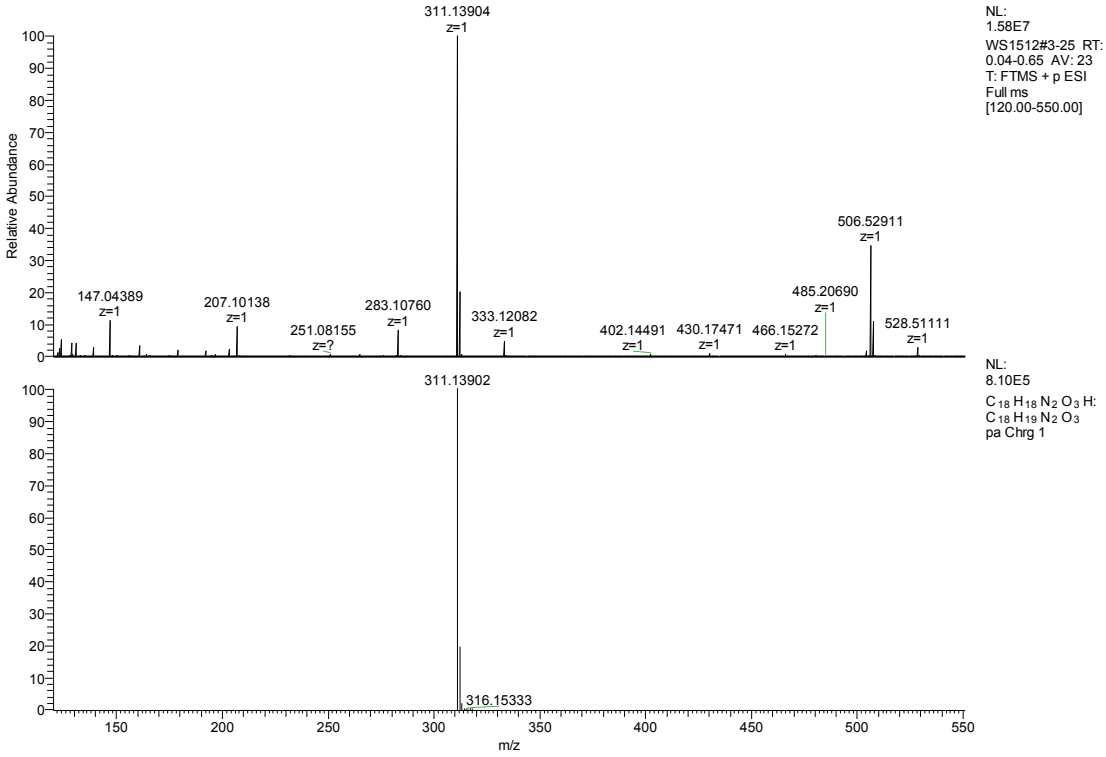

Compound Azo-2 (^{1}H-NMR, 400 MHz, DMSO-d_6)

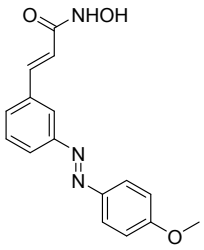

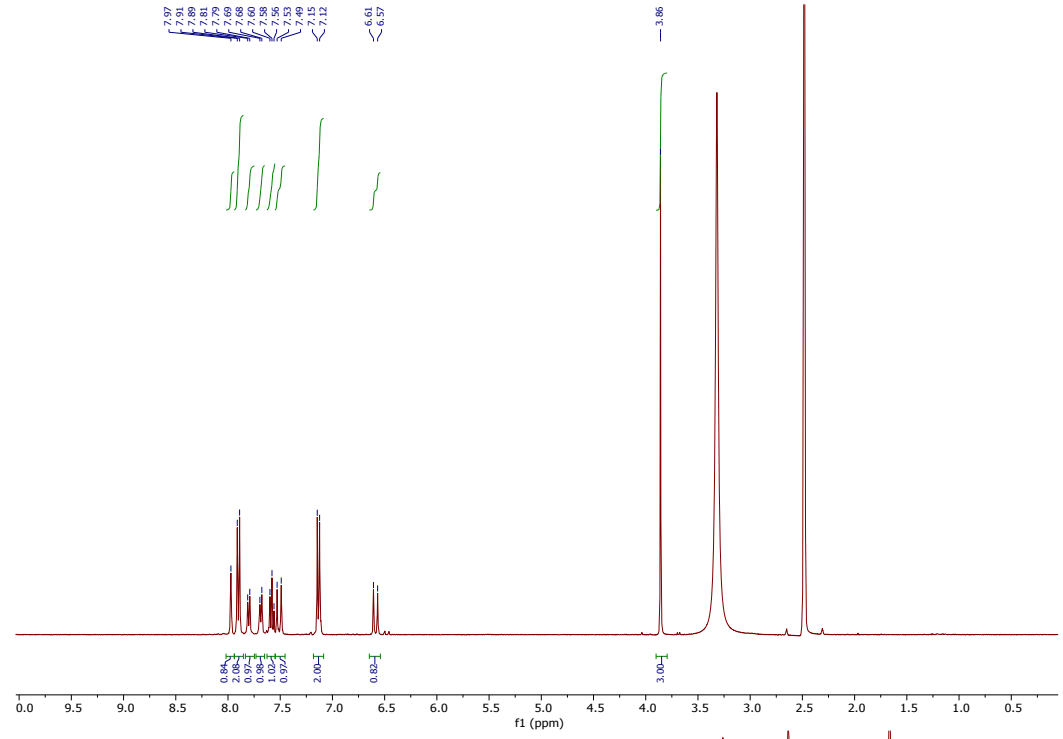

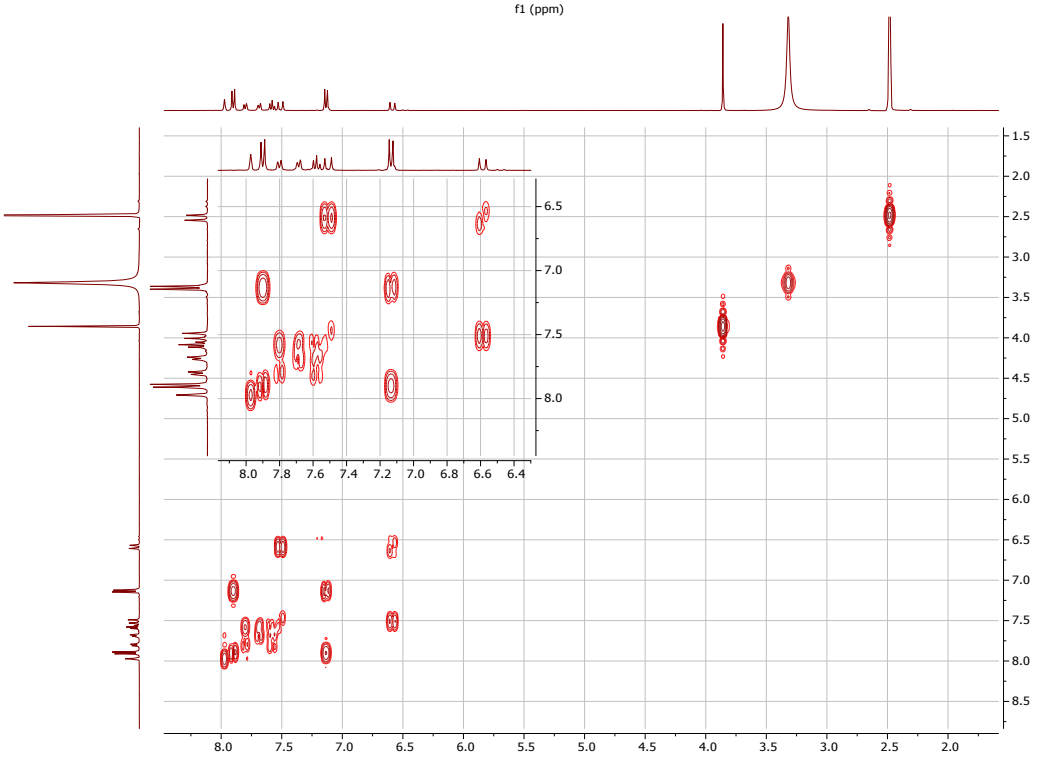

Compound Azo-2 (^{13}C-NMR, 101 MHz, DMSO-d_6)

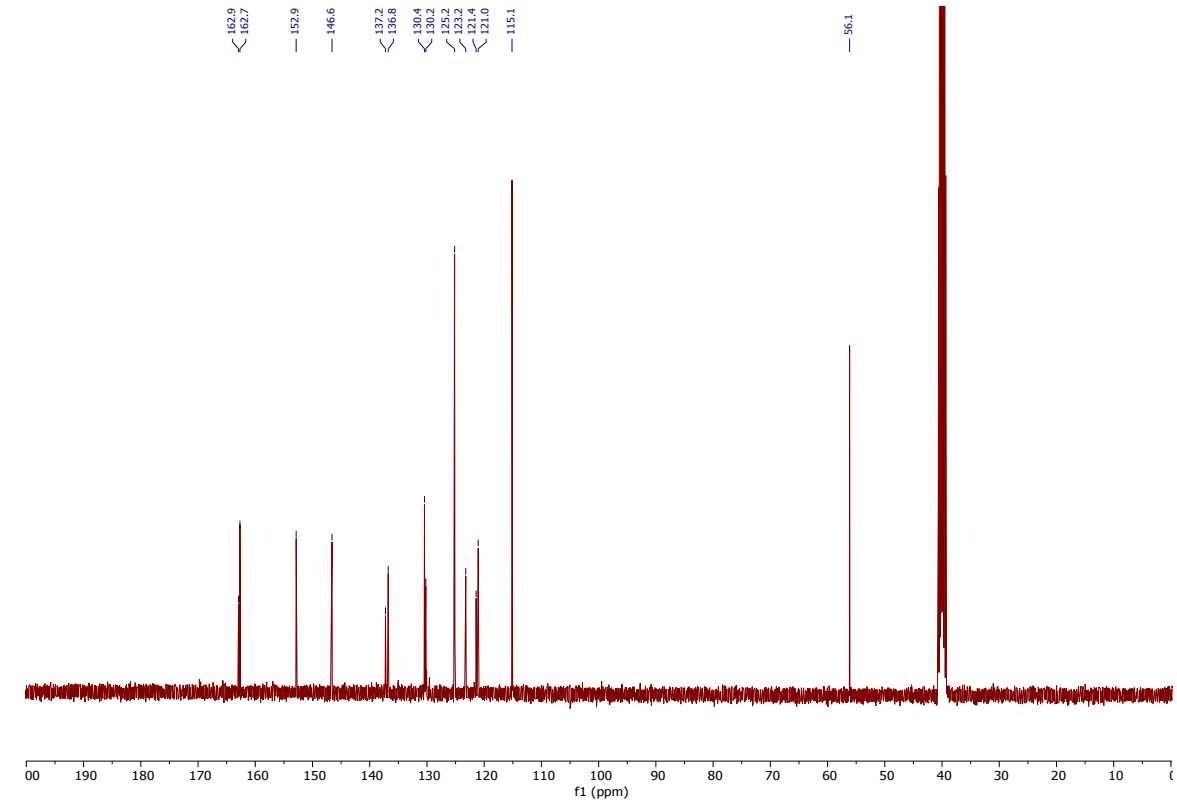

Compound Azo-2 (HRMS)

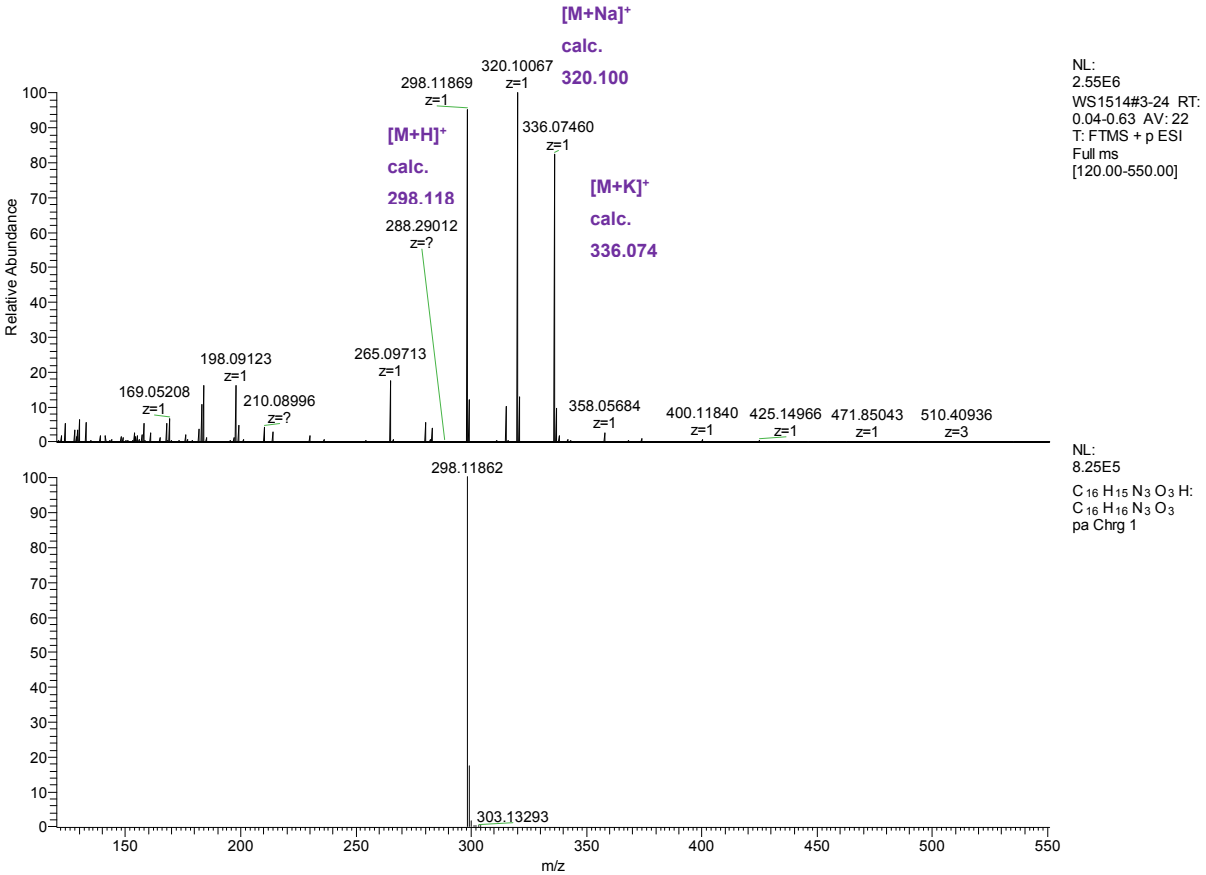

S6. References

1 Q. Liu, F. Huang, X. Yuan, K. Wang, Y. Zou, J. Shen and Y. Xu, *J. Med. Chem.*, 2017, **60**, 10231–10244.

2 F. Tibiletti, M. Simonetti, K. M. Nicholas, G. Palmisano, M. Parravicini, F. Imbesi, S. Tollari and A. Penoni, *Tetrahedron*, 2010, **66**, 1280–1288.

3 H. Fukuda, K. Nishikawa, Y. Fukunaga, K. Okuda, K. Kodama, K. Matsumoto, A. Kano and M. Shindo, *Tetrahedron*, 2016, **72**, 6492–6498.

4 L. Yang, X. Xue and Y. Zhang, *Synth. Commun.*, 2010, **40**, 2520–2524.

5 L. N. Lameijer, S. Budzak, N. A. Simeth, M. J. Hansen, B. L. Feringa, D. Jacquemin and W. Szymanski, *Angew. Chem., Int. Ed.*, 2020, **59**, 21663–21670.

6 P. J. Dockerty, PhD Thesis, University of Groningen, 2018.

7 C. Matera, A. M. J. Gomila, N. Camarero, M. Libergoli, C. Soler and P. Gorostiza, *J. Am. Chem. Soc.*, 2018, **140**, 15764–15773.

8 T. Mashita, T. Kowada, H. Takahashi, T. Matsui and S. Mizukami, *ChemBioChem*, 2019, **20**, 1382–1386.

9 K. Roos, C. Wu, W. Damm, M. Reboul, J. M. Stevenson, C. Lu, M. K. Dahlgren, S. Mondal, W. Chen, L. Wang, R. Abel, R. A. Friesner and E. D. Harder, *J. Chem. Theory Comput.*, 2019, **15**, 1863–1874.

10 W. Sherman, T. Day, M. P. Jacobson, R. A. Friesner and R. Farid, *J. Med. Chem.*, 2006, **49**, 534–553.

11 R. A. Friesner, R. B. Murphy, M. P. Repasky, L. L. Frye, J. R. Greenwood, T. A. Halgren, P. C. Sanschagrin and D. T. Mainz, *J. Med. Chem.*, 2006, **49**, 6177–6196.

12 J. Zhou, R. Wu and H. Bin Luo, *Phys. Chem. Chem. Phys.*, 2015, **17**, 29483–29488.

13 D. Cheshmedzhieva, N. Toshev, M. Gerova, O. Petrov and T. Dudev, *J. Mol. Model.*, 2018, **24**, 2–9.

14 W. L. Jorgensen, J. Chandrasekhar, J. D. Madura, R. W. Impey and M. L. Klein, *J. Chem. Phys.*, 1983, **79**, 926–935.

15 D. E. Shaw, Association for Computing Machinery, New York, NY, USA, 2006.

16 U. Essmann, L. Perera, M. L. Berkowitz, T. Darden, H. Lee and L. G. Pedersen, *J. Chem. Phys.*, 1995, **103**, 8577–8593.

17 H. J. C. Berendsen, J. P. M. Postma, W. F. Van Gunsteren, A. Dinola and J. R. Haak, *J. Chem. Phys.*, 1984, **81**, 3684–3690.

18 G. J. Martyna, D. J. Tobias and M. L. Klein, *J. Chem. Phys.*, 1994, **101**, 4177–4189.

19 D. J. Evans and B. L. Holian, *J. Chem. Phys.*, 1985, **83**, 4069–4074.

20 B. Knapp, L. Ospina and C. M. Deane, *J. Chem. Theory Comput.*, 2018, **14**, 6127–6138.

21 A. D. Bochevarov, E. Harder, T. F. Hughes, J. R. Greenwood, D. A. Braden, D. M. Philipp, D. Rinaldo, M. D. Halls, J. Zhang and R. A. Friesner, *Int. J. Quantum Chem.*, 2013, **113**, 2110–2142.